

Magnetoacoustic Attenuation of Circularly Polarized Ultrasound in Sn, Al, and Sb†*

BARRY I. MILLER††

Department of Physics and Institute for the Study of Metals, The University of Chicago, Chicago, Illinois

(Received 19 May 1966)

The attenuation of circularly polarized sound as a function of magnetic field H , oriented parallel to the sound propagation direction, was measured for Al, Sn, and Sb at 4.2 and 1.2°K. This direction was chosen to be along the [100] axis in Al, the [001] axis in Sn, and the trigonal axis in Sb. The dispersion was also measured in Al and Sn. Doppler-shifted cyclotron resonance, causing peaks and edges in the attenuation, was observed in the case of Al and Sn. For Al the peaks are periodic in $1/H$ with a period of $(1.8 \pm 0.04) \times 10^{-4} \text{G}^{-1}$. These peaks were found to be caused by holes coming from the second Brillouin zone. In Sn both types of carriers contributed to the peaks. Geometric resonance, causing sinusoidal oscillations in the attenuation periodic in $1/H$, was observed in Sb with a period of $(44 \pm 2) \times 10^{-4} \text{G}^{-1}$. This resonance was found to be caused by the hole ellipsoids in Sb. The earlier theories of magnetoacoustic attenuation have been extended to general Fermi surfaces and to include the simultaneous presence of electrons and holes and deformation effects. The relationship between the attenuation and the Fermi surface geometry is discussed for different crystal symmetries and carrier compensations. A comparison between the known Fermi surfaces of Al and Sb and the observed attenuation for these metals is made.

I. INTRODUCTION

MAGNETOACOUSTIC attenuation experiments where the sound propagation vector \mathbf{q} is perpendicular to the magnetic field \mathbf{H} have proved useful in providing a caliper of the Fermi surface of metals.¹⁻⁴ The dependence of the attenuation on a longitudinal magnetic field ($\mathbf{q} \parallel \mathbf{H}$), on the other hand, has been studied in very few metals,⁵⁻¹¹ because the results cannot be interpreted so easily in terms of geometrical parameters of the Fermi surface.¹²⁻¹⁴ Although the

knowledge of Fermi surfaces might not be advanced by such experiments, the longitudinal magnetic field case enables one to study several new and interesting processes concerning the interaction of the conduction electrons with sound waves.

As first discussed by Kjeldaas,¹² Doppler-shifted cyclotron resonance occurs in the longitudinal field case because the carriers drifting with velocity v_z along the field direction see an effective frequency $\omega(v_z/v_s - 1)$ instead of the applied sound frequency ω . Here v_s is the velocity of sound. Denoting the cyclotron frequency by ω_c , the resonance condition is

$$\omega_c = \omega(v_z/v_s - 1) \quad (1.1)$$

or

$$\omega_c = \omega(v_z/v_s + 1), \quad (1.2)$$

depending on whether the carrier is drifting parallel or opposite to the sound velocity. Below a certain magnetic field H_A which is determined by the maximum value of v_z , there will always be some carriers in resonance. The attenuation edge occurring at H_A is known as the Kjeldaas edge.

Not only an edge, but a peak can be observed in the magnetoacoustic attenuation whenever the resonance condition Eq. (1.1) or (1.2) is fulfilled at a given field for a large number of carriers. This happens when $m_c v_z$ or, in other words, $\partial \mathcal{A} / \partial k_z$ is constant over an appreciable part of the Fermi surface. Here m_c is the cyclotron mass, \mathcal{A} is the cross-sectional area of the Fermi surface perpendicular to \mathbf{H} , and k_z is the component of the electron wave vector in the field direction.

Higher harmonics of these edges and peaks in the attenuation are introduced when the Fermi surface does not have full rotational symmetry about the k_z axis. In that case, v_z may become a function of the polar angle ϕ about the z axis and another resonance effect is

¹⁴ J. J. Quinn, Phys. Rev. Letters **11**, 316 (1963); S. G. Eckstein, *ibid.* **16**, 611 (1966).

† Supported by the U. S. Air Force Office of Scientific Research under Contract No. AFOSR 49(638)-1653.

* Submitted in partial fulfillment of the requirements for the degree of Doctor of Philosophy at The University of Chicago, Chicago, Illinois.

† Present address: Bell Telephone Laboratories, Inc., Murray Hill, New Jersey.

¹ For a review of magnetoacoustic effects and a list of recent references see N. Tepley, Proc. IEEE **53**, 1586 (1965).

² M. H. Cohen, M. J. Harrison, and W. A. Harrison, Phys. Rev. **117**, 937 (1960).

³ A. B. Pippard, Proc. Roy. Soc. (London) **A257**, 165 (1960).

⁴ For a discussion of some of these results see *The Fermi Surface*, edited by W. A. Harrison and M. B. Webb (John Wiley & Sons, Inc., New York, 1960), pp. 214-263.

⁵ B. K. Jones, Phil. Mag. **9**, 217 (1964).

⁶ J. B. Ketterson and R. W. Stark, Bull. Am. Phys. Soc. **11**, 90 (1966).

⁷ M. R. Daniel and L. MacKinnon, Phil. Mag. **8**, 537 (1963); L. MacKinnon and M. R. Daniel, Phys. Letters **1**, 159 (1962); L. MacKinnon, M. T. Taylor, and M. R. Daniel, Phil. Mag. **7**, 523 (1962).

⁸ O. Beckman, L. Eriksson, and S. Hornfeldt, Solid State Commun. **2**, 7 (1964).

⁹ A. R. Mackintosh, Phys. Rev. **131**, 2421 (1963).

¹⁰ J. R. Boyd and J. D. Gavenda, Bull. Am. Phys. Soc. **10**, 371 (1965); J. D. Gavenda and J. R. Boyd, Phys. Rev. Letters **15**, 364 (1965); and J. R. Boyd, thesis (unpublished).

¹¹ Some work has also been done for arbitrary angles between \mathbf{q} and \mathbf{H} . See Y. Eckstein, J. B. Ketterson, and S. G. Eckstein, Phys. Rev. **135**, A740 (1964); Y. Eckstein, Bull. Am. Phys. Soc. **11**, 90 (1966); S. G. Eckstein, *ibid.* **11**, 91 (1966); Y. Eckstein, Phys. Letters **20**, 142 (1966) and **20**, 606 (1966); S. G. Eckstein, *ibid.* **20**, 144 (1966); H. N. Spector, Phys. Rev. **120**, 1261 (1960); and H. N. Spector, *ibid.* **125**, 1192 (1962).

¹² T. Kjeldaas, Phys. Rev. **113**, 1473 (1959).

¹³ H. Stolz, Phys. Status Solidi **3**, 1153 (1963); **3**, 1493 (1963); **3**, 1957 (1963); and **9**, 3 (1965).

possible. The ϕ dependence of v_z causes the carriers to oscillate along the z axis as they traverse their orbit. Whenever the amplitude of these spatial oscillations matches the sound wavelength λ , geometric resonance will occur, provided that the velocity averaged over the orbit \bar{v}_z nearly equals v_s , the sound velocity.

Doppler-shifted cyclotron resonance using longitudinal sound waves has been observed in Al⁵ and Mg.⁶ Geometric resonance of this type was observed in Cd⁷ and Sb.⁸

The present investigation involves the use of shear waves. These are of particular interest because of the

following. By restricting ourselves to shear waves traveling along a crystallographic axis of 3-fold or higher rotational symmetry, the normal modes of the sound wave are circularly polarized. By noting the difference in the attenuation as a function of magnetic field between the right-handed (+) and left-handed (-) waves, the sign of the carriers giving rise to the Doppler-shifted cyclotron resonance can be deduced.

Taking into account the possibility of higher harmonics and requiring that the electrons be in phase with the sound wave, the complete cyclotron resonance conditions can be written in two groups:

Type A:

$$\begin{aligned} (-) \text{ wave: } n\omega_c &= \omega(\bar{v}_z/v_s + 1) \Big| n=1, 5, 9 \dots \text{for holes} \\ (+) \text{ wave: } n\omega_c &= \omega(\bar{v}_z/v_s - 1) \Big| n=3, 7, 11 \dots \text{for electrons} \end{aligned} \quad (1.3)$$

Type B:

$$\begin{aligned} (+) \text{ wave: } n\omega_c &= \omega(\bar{v}_z/v_s + 1) \Big| n=3, 7, 11 \dots \text{for holes} \\ (-) \text{ wave: } n\omega_c &= \omega(\bar{v}_z/v_s - 1) \Big| n=1, 2, 9 \dots \text{for electrons.} \end{aligned} \quad (1.4)$$

For a type-A resonance, the attenuation peak or edge for a (+) wave occurs at a slightly larger H than that of (-) wave for the same n . The difference in H is of the order $v_s/v_z n$.

Experiments using shear waves and longitudinal magnetic fields have been carried out on Al,⁵ Sn,⁹ and Cu.¹⁰ However, these experiments used linearly polarized shear waves because of the difficulties involved in detecting circularly polarized shear waves. Besides being unable to distinguish between electrons and holes, experiments with linearly polarized shear waves suffer from uncertainties resulting from the rotation of the plane of polarization similar to Faraday rotation in optics. This may cause some false attenuation peaks when the polarization plane becomes perpendicular to the fixed axis of the receiving transducer.

In this work a method¹⁵ is used which enables one to measure the magnetic field induced change of the attenuation and dispersion of right-handed and left-handed circularly polarized shear waves directly. Such measurements on Sn, Al, and Sb at helium temperatures will be reported. In Sec. IV the existing theories^{2,16-23}

of magnetoacoustic attenuation for parallel fields and shear waves will be extended to general Fermi surfaces and to include deformation-potential terms and the simultaneous presence of electrons and holes.

II. EXPERIMENTAL DETAILS

In the present work the relative attenuation $\alpha^\pm(H) - \alpha(0)$, and dispersion $[q^\pm(H) - q(0)]/q(0)$ of the circularly polarized normal modes for tin and aluminum samples were measured. The relative attenuation for antimony was also measured. When we talk about attenuation (α^\pm) and dispersion ($\Delta q^\pm/q_0$) in the remainder of this paper we always mean these relative quantities.

Circularly polarized sound can only propagate along an axis of threefold or higher symmetry in the presence of a magnetic field parallel to this axis. In tin the sound was propagated along the [001] axis; in aluminum, along the [100] axis; and in antimony, along the trigonal axis.

TABLE I. Sample details.

Sample	Sample length cm	Cross-section area cm ²	Sound propagation direction q	Sound velocity (shear waves) 10 ⁶ cm/sec	Resistance ratio $\rho_{300^\circ\text{K}}/\rho_{4.2^\circ\text{K}}$	$\omega_c \tau^d$ 1 kG
Al	0.47	1.0	[100]	3.40 ^a	5000	0.7
Sb	0.67	2.0	Trigonal	2.43 ^b	6000	85
Sn	0.75	3.0	[001]	1.91 ^c	50 000	2.0

^a G. N. Kamm and H. V. Bohm, Phys. Rev. **131**, 111 (1963).

^b S. Epstein and A. P. DeBretteville, Jr., Phys. Rev. **138**, A771 (1965).

^c J. A. Rayne and B. S. Chandrasekhar, Phys. Rev. **120**, 1658 (1960).

^d This was derived from the 4.2°K resistivity of the metal using the approximation $\sigma = N^2 \tau / m_0$, where N = carrier concentration/cc, and τ is the average relaxation time.

¹⁵ B. I. Miller, Bull. Am. Phys. Soc. **10**, 371 (1965); and B. I. Miller and V. L. Rehn, Rev. Sci. Instr. (to be published).

¹⁶ M. J. Harrison, Phys. Rev. **119**, 1260 (1960).

¹⁷ H. N. Spector, Phys. Rev. **125**, 1880 (1960).

¹⁸ G. L. Kotkin, Zh. Eksperim. i Teor. Fiz. **41**, 281 (1961) [English transl.: Soviet Phys.—JETP **14**, 201 (1962)].

¹⁹ U. P. Silin, Zh. Eksperim. i Teor. Fiz. **38**, 977 (1960) [English transl.: Soviet Phys.—JETP **11**, 703 (1960)].

²⁰ A. E. Kaner, V. G. Peschanskii, and I. A. Privorotskii, Zh. Eksperim. i Teor. Fiz. **40**, 214 (1961) [English transl.: Soviet Phys.—JETP **13**, 147 (1961)].

²¹ K. B. Vlasov and B. N. Filippov, Zh. Eksperim. i Teor. Fiz. **46**, 223 (1964) [English transl.: Soviet Phys.—JETP **19**, 156 (1964)].

²² J. J. Quinn and S. Rodriguez, Phys. Rev. **133**, A1589 (1964); S. Rodriguez, *ibid.* **130**, 1778 (1963).

²³ A. B. Pippard in Ref. 4, pp. 214-263.

The crystals were approximately cubic in shape. Details of the samples are given in Table I. The crystals were grown in a horizontal graphite crucible by passing a molten zone along the length of the crucible at a rate of 1 in. per h. The samples were grown under a vacuum of 10^{-7} – 10^{-8} Torr in order to minimize contamination. The Sn crystal was grown after twenty passes, while the Al and Sb crystals were grown after one pass. The extra passes on the Sn purified it by zone refinement. The results of a mass-spectrometric analysis of the samples is given in Table II.

The samples were aligned by x rays to within $\frac{1}{2}^\circ$. They were cut and planed by spark erosion. The planed surfaces were parallel to within 10^{-4} cm over the transducer area. The depth of the spark erosion pits was about 0.0002 in., and any damage to the crystal was confined to the surface, as confirmed by x-ray analysis.

The method used to propagate and receive circularly polarized sound waves consisted of placing an AC-cut quartz transducer on the front surface of the sample, as shown in Fig. 1. Excitation of this transducer by rf pulses of 3–4- μ sec duration at 60 or 84 MHz simultaneously generates a right- and left-handed circular wave. At the rear surface were placed two AC-cut receiving transducers which had mutually perpendicular displacement axes. The output of one of the receiving transducers was delayed one-fourth period with respect to the other. The two outputs were then added together before rectification. The resulting signal was proportional to either the right or left circularly polarized normal mode.²⁴ Either signal was then amplified and rectified by a logarithmic receiver, after which it went to one axis of an x - y recorder. The attenuation of the right- or left-hand signal (α^+ and α^- , respectively) could be accurately determined to within ± 1 dB over an 80-dB range. The receiving system was sensitive to amplitude changes of 0.0025 dB.

The phase shift of the sound wave going through the sample is $[q^\pm(H) - q(0)]d$, where d is the length of the crystal, and can be determined by comparing the phase of the right- or left-hand signal to that of a fixed refer-

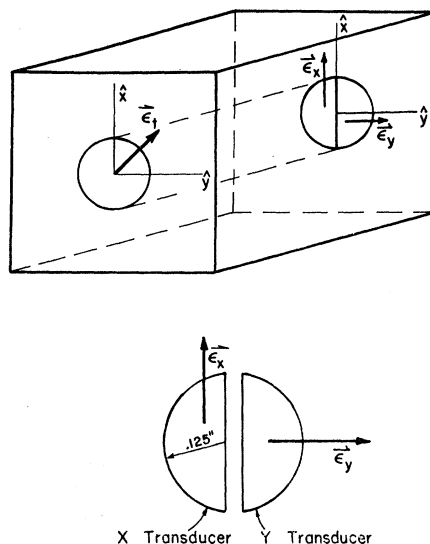


FIG. 1. Transducer geometry used for detecting circularly polarized sound. The transmitting transducer on the front surface is an AC-cut shear transducer whose displacement axis ϵ_x is oriented at 45° with respect to the displacement axes, ϵ_y and ϵ_z , of the receiving transducers on the rear surface.

ence signal. The phase change could be determined to within $\pm 0.05\pi$ rad. The accuracy is limited by the difficulty of getting a good null in the comparison between the signal and reference signal. This, in turn, is limited by the time duration of the signal pulse. In Sec. III a method comparing the direct output of the x and y transducers is shown to give better accuracy in the determination of the dispersion.

The magnetic field was generated by a 0–30-kG superconducting solenoid, having a homogeneity of 0.05% in the sample volume. It is possible to determine the magnetic field by measuring the current through the magnet. However, the field at the sample lags the current when the current is being swept. For example, in a sweep of from 0–6 kG in 15 min, the lag was found to be 200 G. It is possible to correct this by sweeping up and down in field, at the expense of doubling the time for a magnetic-field sweep. This hysteresis effect can be eliminated by use of the Hall probe, except for a very small field lag ≈ 10 G caused by the skin effect of the bulk sample. The Hall probe was mounted directly in the solenoid, near the sample.²⁵ This eliminates significant errors caused by trapped flux at low fields.

The Hall probe used in this work was calibrated at 4.2°K against an NMR probe operating at room temperature. The over-all accuracy in the measurement of H is $\pm 0.5\%$. The sample was aligned parallel to H

TABLE II. Spectrographic analysis.^a

Sample	Impurity ^b ppm								
Sn	Au	Cu	Mn	Cr	Ti	S	Al		
	0.1	0.3	0.01	0.1	0.04	1.0	0.3		
Al	Zn	Fe	K	Cl	Ti	S	Si	Mg	Na
	1.0	1.1	0.4	1.3	0.04	1.0	1.0	0.4	1.0
Sb	As	Fe	K	Cl	Ti	S	Al	Ca	Na
	0.1	0.3	3.5	0.5	0.1	0.3	1.0	3.5	10.0

^a The analysis was done on an Associated Electrical Industries mass spectrometer.

^b Any impurities not listed are presumed to be < 0.01 ppm except for gases which cannot be reliably determined.

²⁴ A wave is defined as right- or left-handed if the displacement vector \mathbf{S} moves in a clockwise or counterclockwise sense, respectively, as viewed from the observer.

²⁵ Two Hall probes were found useful at 4.2°K. International Systems Corporation Hallistor type SV210T is rated for use at 4.2°K, but is fairly nonlinear. Also, after many cycles, it cracked. Hallistor type FC33 is linear to within 0.2% to about 15 kG, but cracks after a few cycles. For other probes see McEvoy and R. F. Decell, Rev. Sci. Instr. 34, 914 (1963).

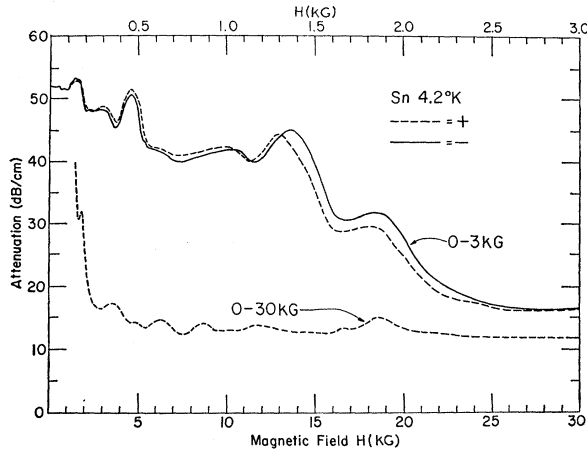


FIG. 2. Attenuation of right- (+) and left-handed (-) waves as a function of H in Sn at 4.2°K. The 0-30-kG curve shows the (+) wave only since the attenuation of the (+) and (-) waves were nearly identical at high magnetic fields.

within $\pm 2^\circ$. Purposely varying the angle of misalignment as much as 5° produced no appreciable change in the results.

III. RESULTS

A. Tin

1. Attenuation

Figure 2 shows the attenuation α^+ and α^- of the right- and left-circularly polarized waves at 4.2°K, respectively, for 84.23 MHz. Only the right-handed wave is plotted for high fields, as the left-handed wave exhibited the same structure and almost the same amplitude.

Most striking in Fig. 2 is the very rapid drop in attenuation over a few thousand gauss. This change in attenuation (40 dB/cm) suggests that a very strong attenuation mechanism takes place at low fields. The decrease in the attenuation as a function of H is suggestive of the Kjeldaa's theory outlined earlier, and the peaks suggest that there are large portions of the Fermi surface for which $m_e \bar{v}_z$ is constant.

The difference in peak positions for the (+) and (-) wave, as given in Eqs. (1.3) and (1.4), is evident near 1350 G, while the peak at 1800 G shows only a small difference, as all the low-field peaks seem to do. As discussed in Sec. I, we can classify these attenuation peaks as belonging to Type A if the (-) peak occurs at higher fields than the (+) peak and Type B if the (+) peak occurs at higher fields than the (-) peak. The peaks near 1350 and 1800 G are of Type A, and if one justifiably assumes that these strong peaks are caused by the fundamental ($n=1$) in the cyclotron frequency, then these peaks are caused by holes.

There appears to be almost no difference in the peak positions of the (+) and (-) waves at 500 G. It is curious, however, that on the high-field side it appears as if the peak were Type B, yet on the low-field side as if it were Type A. This peak is much broader for the

TABLE III. Summary of attenuation peaks from Fig. 4.

Peak number	$H_{av} = (H^+ + H^-)/2$ kG	$H^+ - H^-$ * kG	Peak classification
1	0.453	-0.011 ± 0.002	A
2	0.511	0.014 ± 0.002	B
3	0.585
4	0.657	0.016 ± 0.002	B
5	0.80	0.0 ± 0.003	...
6	0.85	0.0 ± 0.003	...
7	0.90	-0.003 ± 0.003	A
8	0.97	0.0 ± 0.0035	...
9	1.04	-0.018 ± 0.003	A
10	1.33	-0.040 ± 0.002	A
11	1.86	-0.016 ± 0.004	A
12	2.05	-0.009 ± 0.006	A
13	2.26	-0.025 ± 0.006	A
14	2.60	-0.065 ± 0.003	A
15	2.87	-0.040 ± 0.003	A
16	3.07	-0.086 ± 0.006	A
17	3.23	-0.043 ± 0.009	A
18	3.50	0.025 ± 0.009	B
19	3.68	-0.026 ± 0.003	A
20	4.16	-0.031 ± 0.003	A
21	5.03	0.0 ± 0.007	...
22	5.35	0.014 ± 0.007	B
23	5.62
24	6.18	0.086 ± 0.007	B
25	6.70	0.144 ± 0.014	B
26	7.07	-0.014 ± 0.015	A(?)
27	9.03	0.101 ± 0.007	B
28	9.31	0.029 ± 0.020	B
29	10.02	-0.014 ± 0.007	A
30	11.99	0.072 ± 0.025	B
31	16.77	0.058 ± 0.025	B
32	18.47	0.029 ± 0.007	B

* The accuracies quoted apply only to $H^+ - H^-$. This inaccuracy comes from the difficulty in reading the graph and in determining peak maxima. The usual 1% accuracy applies to H_{av} .

(+) wave than for the (-) wave. The field below 300 G is expanded in Fig. 3. Below 200 G there appears to be very little, if any, difference between the (+) and (-) wave.

In order to increase the resolution of the measurements, the attenuation measurements were repeated at 1.2°K. The results are shown in Fig. 4. Many peaks which appeared to be single at 4.2°K show multiple structure at the lower temperature. For example, the peak at 500 G is seen here as a double peak whose high-field side is Type B, and whose low-field side is

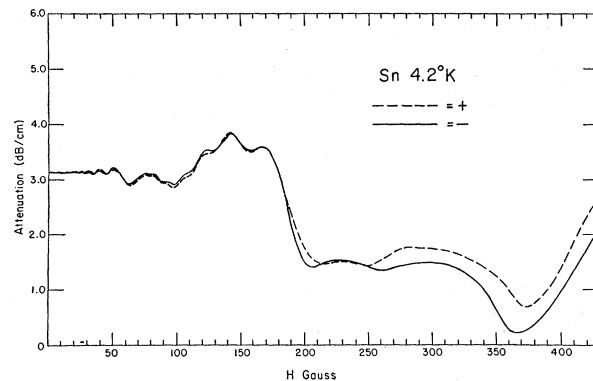


FIG. 3. Attenuation of the right- (+) and left-handed (-) waves in Sn at 4.2°K as a function of H at low magnetic fields.

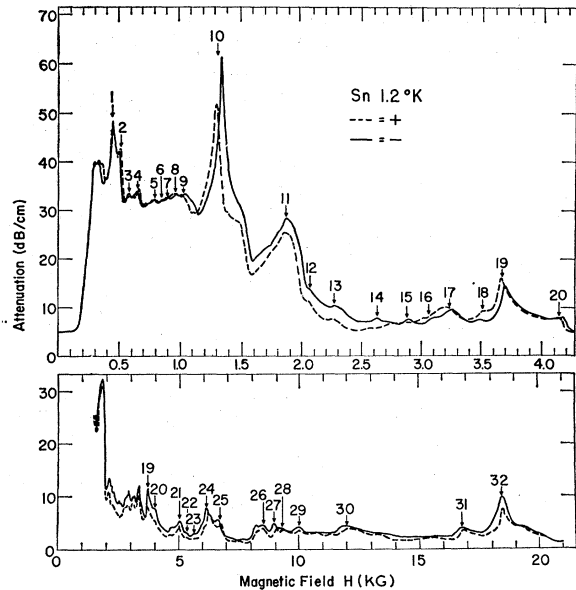


FIG. 4. Attenuation of right- (+) and left-handed (-) waves in Sn at 1.2°K as a function of H . The positions of the peaks as well as their classifications are given in Table III. The sharp drop in the attenuation below 300 G is caused by the onset of superconductivity. Therefore, the peak below number 1 is distorted and is not included in Table III.

Type A. The fact that tin becomes a superconductor in fields below 300 G at 1.2°K accounts for the rapid drop in attenuation below 250 G, in Fig. 4.

The positions of the peaks in Fig. 4, as well as their difference in peak positions for (+) and (-) waves and classifications, are given in Table III. Not included in the table is the peak below peak No. 1, because its low-field side is affected by the rapid decrease in attenuation caused by the onset of superconductivity.

The high-field region shows the attenuation for both (+) and (-) polarizations. Structure in the attenuation curves appears at the very highest of magnetic fields. Above a few kG, however, the attenuation is small compared with the large attenuation found in low fields, and no drastic changes in attenuation occur. This suggests that a strong attenuation mechanism operates at low fields and that a weaker attenuation process persists at the highest fields.

A comparison of measurements at 60 MHz and at 84.23 MHz showed that the positions of all attenuation peaks scale as ω/H . The amplitude of the peaks and the average attenuation level at 60 MHz is less than those at 84.23 MHz. This is expected, since the attenuation at $H=0$ is proportional to $(ql)^n$, where n is between²⁶ 1 and 2 and l is the mean free path of the electrons.

2. Dispersion

In Sec. II it was pointed out that although the dispersion $\Delta q^\pm/q_0$ could be measured directly, these

²⁶ A. B. Pippard, Rept. Progr. Phys. **23**, 176 (1960).

measurements are difficult to perform and also somewhat inaccurate ($\pm 9^\circ$), because of the difficulties involved in making accurate phase measurements using rf pulses. The relative dispersion $[q^+(H) - q^-(H)]/q_0$ can, however, be determined quite easily from the x and y signals.

Figure 5 shows the direct output of the x and y transducers at 4.2°K before the formation of the circular mode. The peaks at 0.5, 1.5, 2.0, and 6.0 kG are caused by the polarization vector \mathbf{S} of the incoming acoustic wave being perpendicular to either the x or y transducers.

We can write the equations for the right- (+) and left-hand (-) waves in the coordinate system of the transducers (see Fig. 1) at any point z along the z axis, as

$$S^+ = \text{Re}\{S_0^+(z)[-i\hat{x} + \hat{y}] \exp[i(q^+z - \omega t)]\}$$

and

$$S^- = \text{Re}\{S_0^-(z)[\hat{x} - i\hat{y}] \exp[i(q^-z - \omega t)]\}, \quad (3.1)$$

where $S_0^\pm(z) = S_0 \exp(-\alpha^\pm z)$. The signal measured by the x and y transducers (which will be referred to as the x and y signals) is the component of S^+ and S^- along the x or y axis, respectively. The absolute value of the x and y signals at a distance d are

$$\begin{aligned} |x| &= ([S_0^+(d)]^2 + [S_0^-(d)]^2 + 2S_0^+(d)S_0^-(d) \sin(2\Delta))^{1/2}, \\ |y| &= ([S_0^+(d)]^2 + [S_0^-(d)]^2 - 2S_0^+(d)S_0^-(d) \sin(2\Delta))^{1/2}, \end{aligned} \quad (3.2)$$

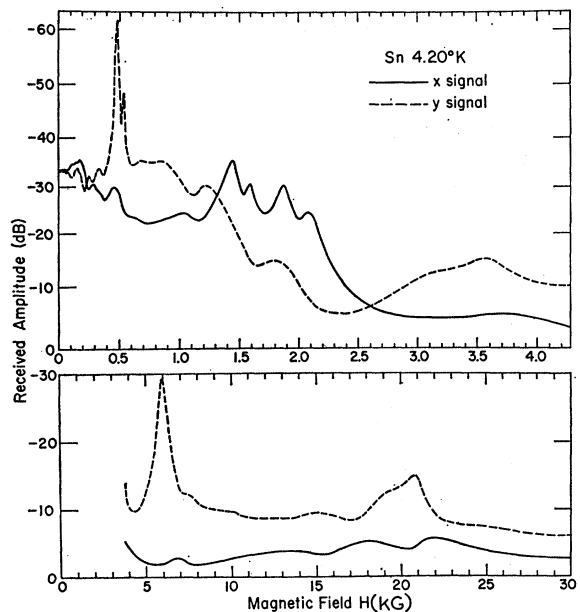


FIG. 5. Direct output of the x and y transducers (see Fig. 1) in Sn at 4.2°K as a function of H . The amplitude of the direct output is plotted in dB with increasingly negative dB values corresponding to decreasing signal amplitudes.

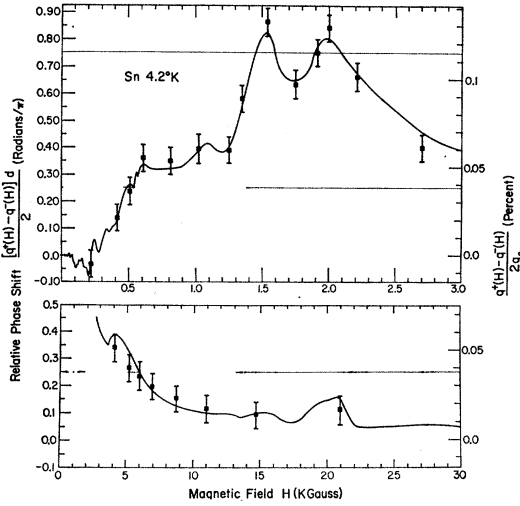


FIG. 6. Phase shift through the sample $[q^+(H) - q^-(H)]d/2$ or dispersion difference $[q^+(H) - q^-(H)]/2$ between the right- (+) and left-handed (-) waves in Sn at 4.2°K as a function of H . The solid line represents the phase shift or dispersion difference as deduced from Fig. 5 and determined by direct measurements (■ points). The light horizontal lines at 0.25π and 0.75π rad set off the different quadrants (see text). By setting $\Delta q^+/q_0 = -\Delta q^-/q_0$, the solid line in Fig. 6 is a plot of $\Delta q^\pm/q_0$ versus H .

where the phase $\Delta = (q^+ - q^-)d/2$. Solving for Δ yields

$$\Delta = \frac{1}{2} \sin^{-1} \left[\frac{1}{2} \left(\frac{S_0^+(d)}{S_0^-(d)} + \frac{S_0^-(d)}{S_0^+(d)} \right) \left(\frac{|x/y| - 1}{|x/y| + 1} \right) \right] + \nu\pi, \quad (3.3)$$

where ν takes on the value $\pm 1, \pm 2, \pm 3, \dots$.

The arbitrary phase factor, $\nu\pi$, in Eq. (3.3), introduces a degree of uncertainty in the determination of Δ .

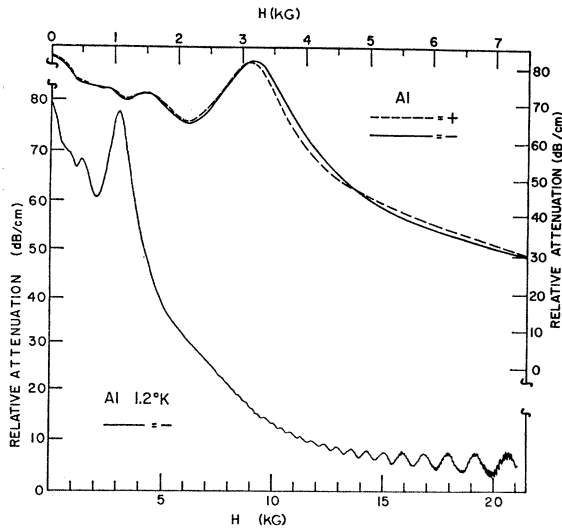


FIG. 7. Attenuation of right- (+) and left-handed (-) waves in Al at 1.2°K as a function of H . The lower curve is plotted only for the (-) wave, since both waves are nearly equal above 7 kG. Except for the high-field quantum oscillations, which are more pronounced at 1.2°K, both curves are identical at 4.2 and 1.2°K.

As Δ increases from 0 to $-\pi/2$, $|y|$ will vanish at $\Delta = -\pi/4$, assuming $S_0^+(d) = S_0^-(d)$. [See Eq. (3.2).] However, if Δ goes from 0 to $-\pi/4$ back to 0, y will still vanish at $\Delta = -\pi/4$. With regard to Fig. 5, the question arises whether the peak at 500 G is caused by Δ going from the $(+\pi/4, -\pi/4)$ quadrant into the $(+\pi/4, +3\pi/4)$ quadrant, or by Δ oscillating in the $(+\pi/4, -\pi/4)$ quadrant. This phase ambiguity can be resolved by changing the length of the sample, by changing the sound frequency, or by direct measurement of the phase change as a function of H .

The accuracy of the direct measurements is sufficient to resolve this phase ambiguity. The solid curve in Fig. 6 represents the phase Δ or Eq. (3.3) after the phase ambiguity has been eliminated by direct measurements.

From the Kjeldaas theory one can show that the following symmetry relationships hold:

$$\alpha^\pm(H) = \alpha^\mp(-H)$$

and

$$\frac{\Delta q^\pm(H)}{q_0} = -\frac{\Delta q^\mp(-H)}{q_0}. \quad (3.4)$$

The relationships are general and hold for arbitrary Fermi surfaces as we will show in Sec. IV. If one neglects the small asymmetry caused by the finite velocity of sound, then $\Delta q^\pm(H) = -\Delta q^\mp(H)$ and hence

$$\frac{\Delta q^\pm(H)}{q_0} = \pm \frac{q^+(H) - q^-(H)}{2q_0}. \quad (3.5)$$

In Fig. 6 we see that the dispersion rises to a plateau between 600 and 1200 G, at which point it rises sharply, forming two peaks centered at 1540 and at 1980 G. The dispersion declines rapidly after these peaks and remains fairly steady above 10 kG. Comparing α^\pm at 4.2°K (Fig. 2) and $\Delta q^\pm/q_0$ at 4.2°K (Fig. 6) shows that the peaks in $\Delta q^\pm/q_0$ occur at the same field where α^\pm changes most rapidly, and the peaks in α^\pm occur when $\Delta q^\pm/q_0$ changes most rapidly.²⁷

²⁷ It appears as if $\Delta q^\pm(H)/q_0$ is related to $\alpha^\pm(H)$ by a dispersion relationship in H such as the Kramers-Kronig transformations. We applied the Kramers-Kronig transformations to $\alpha^\pm(H)$ (Fig. 2) and obtained a curve which appeared almost identical to $\Delta q^\pm(H)/q_0$ (Fig. 6) above 800 G, but below 800 G appears almost opposite to Fig. 6, i.e., the peaks in the inversion corresponded to valleys in the $\Delta q^\pm(H)/q_0$ curve. It was pointed out to us by Dr. V. Heine that the electrons or holes may obey opposite dispersion relationships corresponding to closing the contour for the dispersion integrals in the upper or lower half-planes. He also went on to show that if peaks number 1, 5, 9, ... etc., for a certain carrier belong to one contour, then peaks number 3, 7, 11, ... etc., belong to the opposite contour. The reason that this ambiguity is avoided in Kramers-Kronig transformations in ω is because of the causality principle which limits the contour to the upper half-plane.

Using these Kramers-Kronig transformations may prove useful in analyzing this type of data, but because of the complexity of our data, we were unable to take advantage of this.

B. Aluminum

1. Attenuation

In Fig. 7, α^+ and α^- are plotted as a function of H from 0–7.5 kG at 1.2°K. The results are the same at 4.2°K. The high-field plot from 0–20 kG shows only α^+ , since $\alpha^+ = \alpha^-$ above 6 kG. In Fig. 7 an H dependence, similar in some respects to that observed in tin, is seen. At low magnetic fields the attenuation is high, dropping off to a relatively constant value above a certain field (4 kG). It remains relatively constant at high fields.

The rapid oscillations in the region above 10 kG are quantum oscillations²⁸ (de Haas–Schubnikov) and are unrelated to Doppler-shifted cyclotron resonance and geometric resonance. Both sets of quantum oscillations are periodic in $1/H$ with periods of $(3.62 \pm 0.006) \times 10^{-6} \text{ G}^{-1}$, and $(2.71 \pm 0.003) \times 10^{-7} \text{ G}^{-1}$, respectively. This agrees well with the work of Gunnerson,²⁹ who used the torque method and found the periods $(3.61 \pm 0.13) \times 10^{-6} \text{ G}^{-1}$ and $(2.58 \pm 0.005) \times 10^{-7} \text{ G}^{-1}$. These oscillations are due to the electron “arms” in the third

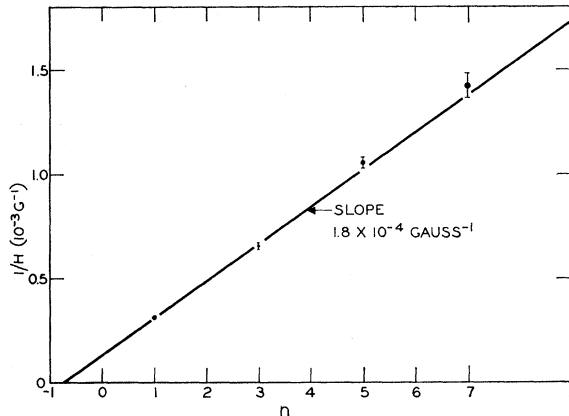


FIG. 8. Plot of $1/H_I$ versus peak number I in Al at 1.2°K, taken from Fig. 7. For attenuation arising from the second zone of Al, I takes on the values 1, 3, 5, ... (see text).

zone of aluminum. The oscillations from the holes in the second zone are expected to appear above 50 kG,³⁰ and for this reason they do not appear in Fig. 7.

In aluminum, as with tin, there is structure below the edge at 4 kG. However, since the Fermi surface of aluminum has only two sheets³¹ compared with five for tin,^{32,33} the structure in Fig. 7 is far less complicated

²⁸ These quantum oscillations in the magnetoacoustic attenuation were first noticed by D. Reneker, Phys. Rev. **115**, 303 (1959) in bismuth. For a list of more recent work see Ref. 1.

²⁹ E. M. Gunnerson, Phil. Trans. Roy. Soc. London **A249**, 299 (1957).

³⁰ M. G. Priestley, Phil. Mag. **7**, 1205 (1962).

³¹ W. A. Harrison, Phys. Rev. **118**, 1182 (1960); N. W. Ashcroft, Phil. Mag. **8**, 2055 (1963); see also Refs. 28 and 29.

³² G. Weisz, Phys. Rev. **149**, 504 (1966).

³³ For the free-electron model of tin, see A. V. Gold and M. G. Priestley, Phil. Mag. **5**, 1089 (1960); V. F. Gantmakher, Zh. Eksperim. i Teor. Fiz. **44**, 811 (1963); **46**, 2028 (1964) [English transl.: Soviet Phys.—JETP **17**, 549 (1963); **19**, 1366 (1964)]; and V. F. Gantmakher and E. A. Kaner, Zh. Eksperim. i Teor. Fiz. **45**, 1430 (1963) [English transl.:—JETP **18**, 988 (1964)].

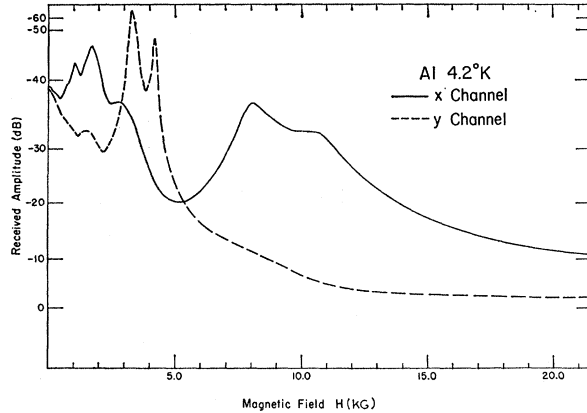


FIG. 9. Direct output of the x and y transducers (see Fig. 3) in Al at 4.2°K as a function of H . The amplitude of the direct output is plotted in dB with increasingly negative dB values corresponding to decreasing amplitudes. Except for quantum oscillations these curves are identical at 1.2°K.

than that in Figs. 2 and 4. The peaks in Fig. 7 appear to belong to one family, since their amplitude decreases at lower fields, as would be expected for higher harmonics of the Doppler-shifted cyclotron resonance.

As seen in Fig. 8, the peaks are nearly periodic in $1/H$ with a slope of $(1.80 \pm 0.04) \times 10^{-4} \text{ G}^{-1}$. The resonance is expected to occur only for the 1, 3, 5, etc., harmonics, and for this reason the peaks are assigned these values in Fig. 8. Since peaks 1 and 5 are of Type A [the (–) wave leads the (+) wave in H] and 3 and 7 are of Type B, we conclude that these peaks are due to the holes in the second zone. The holes are expected to dominate because they are the majority carriers.

2. Dispersion

The direct signals from the x and y transducers are shown in Fig. 9. These data were taken at 4.2°K and are identical with the results obtained at 1.2°K. The peak near 2 kG, the double peak near 4 kG, and the

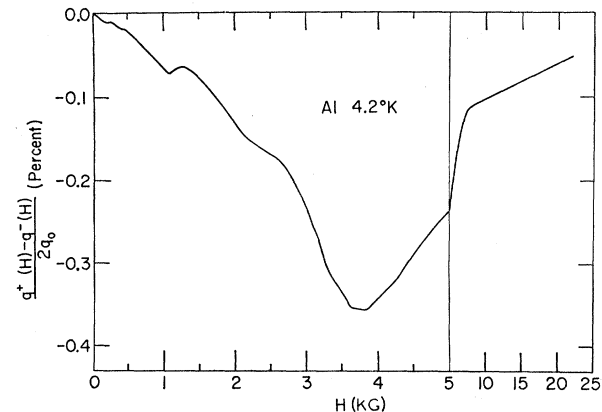


FIG. 10. Dispersion difference $[q^+(H) - q^-(H)]/2q_0$ between the right- (+) and left-handed (–) waves in Al at 4.2°K as a function of H . By setting $\Delta q^+/q_0 = -\Delta q^-/q_0$, this becomes a plot of $\Delta q^\pm/q_0$ versus H .

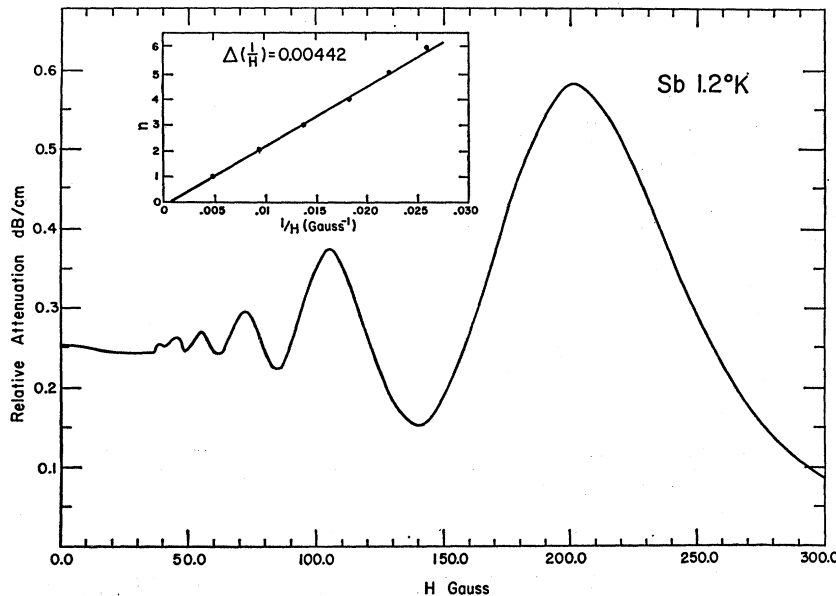


FIG. 11. Average attenuation $(\alpha^+ + \alpha^-)/2$ of Sb at 1.2°K as a function of H . Above 300 G the curve flattens out, remains steady up to 20 kG. The inset shows the peak positions in $1/H$ plotted versus peak number. Here the peaks are numbered consecutively because they are caused by geometric resonance (see text).

peak near 8 kG are points where the phase $[q^+(H) - q^-(H)]d$ might be changing quadrants. The phase ambiguity was again resolved by direct measurements. The dispersion, $(q^+ - q^-)/2q_0$, is shown in Fig. 10. Since the sound velocity is much smaller than the components of the electron velocity parallel to H of the orbits contributing to the attenuation peaks, Eq. (3.5) can be assumed to be valid. As in the case of tin, the positions of peaks and slopes of the α^\pm and $\Delta q^\pm/q_0$ curves are interrelated.

C. Attenuation in Antimony

Antimony is compensated semimetal with about 10^{-3} carriers per atom.^{34,35} Because of the small carrier concentration, the magnetoacoustic attenuation of Sb is much smaller than that in normal metals. We believe that the major contribution to the attenuation in Sb is due to very small pockets in momentum space of electrons and holes,³⁴⁻³⁸ which are very sensitive to the deformation induced by the acoustic wave. This will be discussed in Sec. V.

The small magnitude of the attenuation made it necessary to pass the sound pulse five times through the length of the sample before detection. The difficulties involved with the reflections made it impossible to preserve the mode characteristic.³⁹ If the direct out-

puts of the x and y transducers are identical, as was found in the case of antimony, then either signal yields $(\alpha^+ + \alpha^-)/2$ and the rotation of the plane of polarization is negligible. This average attenuation measured at 84.23 MHz is plotted in Fig. 11. The attenuation begins at some low value, oscillates about this value as H is increased, and then stays constant up to 20 kG.

The oscillations are periodic in $1/H$ with a periodicity of $0.00442 \pm 0.0002 \text{ G}^{-1}$. This value agrees with the value of 0.0046 G^{-1} which was obtained by Beckman *et al.*,⁸ who used longitudinal waves instead of transverse waves but otherwise the same geometry. Beckman attributes these oscillations to geometric resonance of the kind discussed earlier. He was able to show that the oscillations arose from the tilted ellipsoids in antimony. The numerical agreement indicates strongly that the experiments with longitudinal and with transverse waves detect the same effect. This will be analyzed in detail in Sec. V.

IV. THEORY

Some of the effects which have been observed can be understood by generalizing the Kjeldaa's theory, taking into account general Fermi surfaces with many sheets, as well as the simultaneous presence of electrons and holes. In the following discussion we will treat only closed surfaces and will neglect magnetic breakdown.

Following Kjeldaa's¹² and others,¹⁸⁻²² the wave equation for sound in a crystal in the presence of a magnetic field is

$$\partial^2 \mathbf{S} / \partial t^2 = v_s^2 \nabla^2 \mathbf{S} + \mathbf{F} / M, \quad (4.1)$$

where M is the ionic mass, and \mathbf{F} is the damping force acting on one ion and is responsible for the attenuation and dispersion. This force arises from the self-consistent electric field \mathbf{E} , the magnetic field \mathbf{H} , and two additional forces, \mathbf{F}_e and \mathbf{F}_D . One of these forces, \mathbf{F}_e , coherently

³⁴ J. Ketterson and Y. Eckstein, *Phys. Rev.* **132**, 1885 (1963); S. J. Freedman and H. J. Juretschke, *ibid.* **124**, 1379 (1961).

³⁵ L. R. Windmiller, *Phys. Rev.* **149**, 472 (1966).

³⁶ L. M. Falicov and P. J. Lin, *Phys. Rev.* **141**, 562 (1966).

³⁷ Y. Eckstein, *Phys. Rev.* **129**, 12 (1963); J. Ketterson, *ibid.* **129**, 18 (1963); W. R. Datars and R. N. Dexter, *ibid.* **124**, 75 (1961); W. R. Datars, *Can. J. Phys.* **40**, 1984 (1962).

³⁸ D. Shoenberg, *Phil. Trans. Roy. Soc. London* **A245**, 1 (1952).

³⁹ Some of the difficulties involved are: (1) the (+) mode may become a (-) mode upon reflection, depending on the reflection coefficients, and (2) the reflection coefficients may be sensitive to changes in H , while the transmission coefficient is not.

feeds energy back into the ion system because of collisions between the electrons or holes and the ions. The other force, \mathbf{F}_D , can be related to the energy lost in distorting the Fermi surface and depends upon the deformation potential.

The force \mathbf{F} can be written as

$$\mathbf{F} = Ze\boldsymbol{\varepsilon} + Z(e/c)\mathbf{u} \times \mathbf{H} + \mathbf{F}_e + \mathbf{F}_D = \mathbf{A} \cdot \mathbf{u}, \quad (4.2)$$

where $\mathbf{u} = d\mathbf{S}/dt$ is the ion velocity and Z is determined by the condition for charge neutrality

$$ZN = N_e - N_h, \quad (4.3)$$

where the quantity N is the number of ions per unit volume. Equation (4.3) is valid if no magnetic breakdown occurs, and if the sheets of the Fermi surface with N_e electrons and N_h holes per cc, respectively, are energetically separated from each other as well as from all other bands. The relation $\mathbf{F} = \mathbf{A} \cdot \mathbf{u}$ assumes that $\boldsymbol{\varepsilon}$, \mathbf{F}_e , and \mathbf{F}_D are proportional to \mathbf{u} , thus we are restricting ourselves to effects proportional to \mathbf{u} in first order.

By inserting Eq. (4.2) into Eq. (4.1) and setting $\mathbf{q} \parallel \mathbf{H} \parallel \hat{z}$, we obtain the solution of Eq. (4.1) for circular waves to first order in $A^\pm/\omega M$;

$$Q^\pm(H) = q_0[1 + i(A^\pm/2\omega M)], \quad (4.4)$$

where $q_0 = \text{Re}(Q(0))$ is the sound propagation constant at zero magnetic field⁴⁰ and the complex propagation constant Q^\pm is defined by $u^\pm = u_0^\pm \exp[i(Q^\pm Z - \omega t)]$. In circular coordinates $u^\pm = u_x \pm iu_y$ and $A^\pm = A_{xx} \pm iA_{yx}$. The attenuation α^\pm and dispersion $\Delta q^\pm/q_0$ are given by

$$\alpha^\pm = \text{Im}[Q^\pm(H) - Q(0)] \\ = (q_0/2M\omega) \text{Re}[A^\pm(H) - A^\pm(0)] \quad (4.5)$$

and

$$\frac{\Delta q^\pm}{q_0} = \text{Re}\left[\frac{Q^\pm(H) - q_0}{q_0}\right] = -\frac{1}{2M\omega} \text{Im}[A^\pm(H) - A^\pm(0)], \quad (4.6)$$

respectively.

A. Self-Consistent Field

Equation (4.2) shows that A^\pm depends on the quantities $\boldsymbol{\varepsilon}$, \mathbf{F}_e , and \mathbf{F}_D , which can be derived by following the procedures given by Cohen, Harrison, and Harrison,² M. Harrison,¹⁶ and Spector.¹⁷

The self-consistent field $\boldsymbol{\varepsilon}$ can be determined by combining the Boltzmann equation, giving the total electronic current density $j_e + j_h$, with the relation

$$\mathbf{j}_e + \mathbf{j}_h + ZeN\mathbf{u} = -\sigma_0\mathbf{B} \cdot \boldsymbol{\varepsilon} \quad (4.7)$$

as derived by Cohen *et al.*² from Maxwell's equations.

⁴⁰ The quantity q_0 as used in Eq. (4.4) is not strictly equal to $\text{Re}(Q^\pm(0))$, since $\text{Im}(A^\pm)$, which accounts for the ac (i.e., $\omega \neq 0$) electronic contribution to the dispersion, contains terms which do not vanish at zero magnetic field. To be precise q_0 should be replaced by q_{static} in Eq. (4.4), where q_{static} is the sound propagation constant in the limit as $\omega \rightarrow 0$. The difference between q_{static} and q_0 is of the order of a few percent or less as determined by noting the change in the sound velocity between 300 and 4.2°K.

The tensor \mathbf{B} is

$$\mathbf{B} = \begin{pmatrix} i\beta & 0 & 0 \\ 0 & i\beta & 0 \\ 0 & 0 & -i\gamma \end{pmatrix},$$

where $\beta = \omega c^2/4\pi\sigma_0 v_s^2$, $\gamma = \beta(v_s/c)^2$, and σ_0 is the dc conductivity. The screening parameter β is proportional to the square of the ratio of the classical skin depth to the sound wave length. For perfect screening β would equal zero. In Al and Sn at 4.20°K at 84 MHz $\beta \approx 10^{-4}$.

The currents j_e and j_h are defined as

$$\mathbf{j}_e = -e \int \mathbf{v} f_e d\mathbf{k}, \quad (4.8)$$

$$\mathbf{j}_h = e \int \mathbf{v} f_h d\mathbf{k},$$

where f_e and f_h are the distribution functions for electrons and holes having velocity \mathbf{v} , and position \mathbf{r} . In this case we assume a single electron sheet and a single hole sheet. The results can readily be extended to many sheets.

The quantities f_e and f_h can be derived from the Boltzmann equation if one knows the energy expressions for electrons and holes in the presence of a sound wave. Following Harrison and Spector, these energies can be written as

$$E_e(\mathbf{k}) = E_e^0(\mathbf{k}) - (\mathbf{q} \cdot \mathbf{V}_e(\mathbf{k}) \cdot \mathbf{u})/\omega, \\ E_h(\mathbf{k}) = E_h^0(\mathbf{k}) - (\mathbf{q} \cdot \mathbf{V}_h(\mathbf{k}) \cdot \mathbf{u})/\omega, \quad (4.9)$$

where $\mathbf{V}_e(\mathbf{k})$ and $\mathbf{V}_h(\mathbf{k})$ are the deformation potential tensors for electrons or holes at a given point \mathbf{k} in the Brillouin zone, and $E_e^0(\mathbf{k})$ and $E_h^0(\mathbf{k})$ are the electron and hole energies in the absence of a sound wave.

Solving the Boltzmann equation by the path integral method of Chambers,⁴¹ the distribution functions f_e and f_h are found to be

$$f_p = -\frac{\partial f_p^0}{\partial E} \int_{-\infty}^t \mathbf{v}' \cdot \left[g e \boldsymbol{\varepsilon}' + \frac{m\mathbf{u}'}{\tau_p} - \frac{\mathbf{q}(\mathbf{q} \cdot \mathbf{V}_p \cdot \mathbf{u}')}{i\omega} \right] \\ \times \exp\left(\frac{t' - t}{\tau_p}\right) dt'. \quad (4.10)$$

The quantities \mathbf{u}' and $\boldsymbol{\varepsilon}'$ vary as $\exp[i(\mathbf{q} \cdot \mathbf{r}' - \omega t')]$ in the presence of a sound wave. By making the substitution $\phi = \omega t'$, where ϕ is the polar angle about the k_z axis, Eq. (4.10) can be rewritten as

$$f_p = -\frac{\partial f_p^0}{\partial E} \int_{-\infty}^{\phi} \frac{\mathbf{v}'}{\omega_{cp}} \cdot \left[g e \boldsymbol{\varepsilon} + \frac{m\mathbf{u}}{\tau_p} - \frac{\mathbf{q}(\mathbf{q} \cdot \mathbf{V}_p \cdot \mathbf{u})}{i\omega} \right] \\ \times K_p(\phi, \phi') d\phi', \quad (4.11)$$

where

$$K_p(\phi, \phi') = \exp\left[\int_{\phi'}^{\phi} d\phi'' \left(i \frac{\mathbf{q} \cdot \mathbf{v}'' - \omega}{\omega_{cp}} + \frac{1}{\omega_{cp}\tau_p} \right) \right]. \quad (4.12)$$

⁴¹ R. G. Chambers, Proc. Roy. Soc. (London) A65, 458 (1952).

The quantities $\boldsymbol{\varepsilon}$ and \mathbf{u} are in the unprimed coordinate system. In Eqs. (4.10), (4.11), and (4.12), the quantity p stands for either electrons (e) or holes (h), and $g = \pm 1$ for holes and electrons, respectively. The quantity f_p^0 is the unperturbed distribution function, and τ_p is the particle relaxation time. The term $m\mathbf{u}/\tau_p$ accounts for collision drag, as discussed by Holstein.⁴² The mass m is the free-electron mass.

As we are only interested in the attenuation and dispersion of shear waves, a diffusion term accounting for longitudinal currents need not be included in Eq. (4.10) or (4.11).

In general, $\mathbf{V}_p(\mathbf{k})$ depends on \mathbf{k} and cannot be taken out of the integral in Eq. (4.11). Likewise, the relaxation time may depend on \mathbf{k} . However, by assuming that $\tau_p(\mathbf{k})$ is nearly a constant for a given sheet of the Fermi surface,⁴³ τ_p can be removed from the integral in Eq. (4.11). Using Eqs. (4.11) and (4.8), the current can be written as

$$\begin{aligned} \mathbf{j}_e &= \sigma_e \cdot (\boldsymbol{\varepsilon} - m\mathbf{u}/e\tau_e) + \mathbf{D}_e \cdot \mathbf{u}, \\ \mathbf{j}_h &= \sigma_h \cdot (\boldsymbol{\varepsilon} + m\mathbf{u}/e\tau_h) - \mathbf{D}_h \cdot \mathbf{u}, \end{aligned} \quad (4.13)$$

where

$$\sigma_p = e^2 \int \left(-\frac{\partial f_p^0}{\partial E} \right) v d\mathbf{k} \int_{-\infty}^{\phi} \left(\frac{\mathbf{v}'}{\omega_{cp}} \right) K_p(\phi, \phi') d\phi'. \quad (4.14)$$

The integral over ϕ' in Eq. (4.14) is the path integral of the electron or hole at a given velocity \mathbf{v} . It is then integrated over k space. The tensor \mathbf{D}_p is defined as

$$\begin{aligned} \mathbf{D}_p &= e^2 \int \left(-\frac{\partial f_p^0}{\partial E} \right) v d\mathbf{k} \int_{-\infty}^{\phi} \frac{1}{\omega_{cp}} \left(\frac{\mathbf{q} \cdot \mathbf{V}_p'}{i\omega e} \right) \mathbf{q} \\ &\quad \cdot \mathbf{v}' K_p(\phi, \phi') d\phi'. \end{aligned} \quad (4.15)$$

Using Eqs. (4.7) and (4.13), the self-consistent field is

$$\boldsymbol{\varepsilon} = -[\sigma_e + \sigma_h + \mathbf{B}\sigma_0]^{-1} \cdot \left\{ \left[ZNe - \frac{m\sigma_e}{e\tau_e} + \frac{m\sigma_h}{e\tau_h} + \mathbf{D}_e + \mathbf{D}_h \right] \cdot \mathbf{u} \right\}. \quad (4.16)$$

B. Coherent Force F_c

The coherent force arises because the average electron or hole velocity, $\langle \mathbf{v}_e \rangle$ and $\langle \mathbf{v}_h \rangle$, before collision differs from their average velocity, \mathbf{u} , after collision, causing a net transfer of momentum to the lattice. In the case of multiple electron and hole sheets, $\langle \mathbf{v}_e \rangle$ and $\langle \mathbf{v}_h \rangle$ would be the average electron and hole velocities for the whole metal.

Following Harrison,¹⁶ the expression for the coherent force can be written as

$$\mathbf{F}_c = -\frac{m N_e}{\tau_e N} \langle \langle \mathbf{v}_e \rangle - \mathbf{u} \rangle + \frac{m N_h}{\tau_h N} \langle \langle \mathbf{v}_h \rangle - \mathbf{u} \rangle. \quad (4.17)$$

⁴² T. Holstein, Phys. Rev. **113**, 479 (1959).

⁴³ The anisotropic relaxation time $\tau(\mathbf{k})$ could be kept within the integral [Eq. (5.11)] and \mathbf{D} redefined to include both \mathbf{v} and $(1/\tau(\mathbf{k}))\mathbf{I}$, where \mathbf{I} is a unit tensor.

The quantities $\langle \mathbf{v}_e \rangle$ and $\langle \mathbf{v}_h \rangle$ are defined by $\mathbf{j}_e = -N_e e \langle \mathbf{v}_e \rangle$ and $\mathbf{j}_h = N_h e \langle \mathbf{v}_h \rangle$. Hence, Eq. (4.17) can be rewritten as

$$\begin{aligned} \mathbf{F}_c &= -\frac{m}{N} \left(\frac{N_e}{\tau_e} + \frac{N_h}{\tau_h} \right) \mathbf{u} + \frac{m}{2eN} (\mathbf{j}_h + \mathbf{j}_e) \left(\frac{1}{\tau_h} - \frac{1}{\tau_e} \right) \\ &\quad + \frac{m}{2eN} (\mathbf{j}_h - \mathbf{j}_e) \left(\frac{1}{\tau_h} + \frac{1}{\tau_e} \right). \end{aligned} \quad (4.18)$$

Using Eqs. (4.7) and (4.13) the coherent force \mathbf{F}_c becomes

$$\begin{aligned} \mathbf{F}_c &= -\frac{m}{N} \left[\left(\frac{N_e}{\tau_e} + \frac{N_h}{\tau_h} \right) \mathbf{I} + \frac{ZN}{2} \left(\frac{1}{\tau_h} - \frac{1}{\tau_e} \right) \mathbf{I} \right. \\ &\quad \left. - \frac{1}{2e} \left(\frac{1}{\tau_h} + \frac{1}{\tau_e} \right) \left(\frac{m}{e\tau_h} \sigma_h + \frac{m}{e\tau_e} \sigma_e - \mathbf{D}_h - \mathbf{D}_e \right) \right] \cdot \mathbf{u} \\ &\quad + \frac{m}{2Ne} \left[-\left(\frac{1}{\tau_h} - \frac{1}{\tau_e} \right) \sigma_0 \mathbf{B} + \left(\frac{1}{\tau_h} + \frac{1}{\tau_e} \right) (\sigma_h - \sigma_e) \right] \cdot \boldsymbol{\varepsilon}, \end{aligned} \quad (4.19)$$

where \mathbf{I} is the unit tensor.

For metals having only electrons or only holes,

$$\mathbf{F}_c = -gZe \left(\sigma_0 / \left(\frac{ZN e^2 \tau_p}{m} \right) \right) \mathbf{B} \cdot \boldsymbol{\varepsilon}$$

will give only a small contribution to Eq. (4.2) since $\sigma_0 / (ZN e^2 \tau_p / m) \approx 1$ and $\beta \approx 10^{-4}$. Only when electrons or holes are simultaneously present does \mathbf{F}_c add a significant contribution to Eq. (4.2).

C. Deformation Force F_D

From the Boltzmann equation Harrison and Spector were able to show that the force on a carrier due to the distortion of the Fermi surface by the sound wave is

$$\mathbf{q}(\mathbf{q} \cdot \mathbf{V}_p \cdot \mathbf{u}) / i\omega.$$

The power taken from the lattice by the motion of the carriers under this deformation force is

$$p = (1/i\omega) \int \mathbf{q}(\mathbf{q} \cdot \mathbf{V}_p \cdot \mathbf{u}) \cdot \mathbf{v} f_p d\mathbf{k}.$$

The integration averages the power over the particle distribution, where f_p is the distribution function defined in Eq. (4.10). This power represents a complex flow of energy from the sound wave into the electron system and is equal to $\mathbf{F}_D \cdot \mathbf{u}$, where \mathbf{F}_D is the force on the ions accounting for the power lost in deforming the Fermi surface. Solving for the force \mathbf{F}_D , we get

$$\mathbf{F}_D = (1/N) \int [(\mathbf{q} \cdot \mathbf{V}_p) / i\omega] (\mathbf{q} \cdot \mathbf{v}) f_p d\mathbf{k}. \quad (4.20)$$

Using Eq. (4.11), \mathbf{F}_D can be written as

$$\mathbf{F}_D = (\mathbf{D}_h' - \mathbf{D}_e') \frac{\boldsymbol{\varepsilon}}{N} + \left(\frac{m}{e\tau_e} \mathbf{D}_e' + \frac{m}{e\tau_h} \mathbf{D}_h' \right) \cdot \mathbf{u} + (\boldsymbol{\Lambda}_e + \boldsymbol{\Lambda}_h) \cdot \frac{\mathbf{u}}{N}, \quad (4.21)$$

where

$$\mathbf{D}_p' = \frac{e}{i\omega} \int \frac{\mathbf{q} \cdot \mathbf{v}}{\omega_{ep}} (\mathbf{q} \cdot \mathbf{V}_p) \left(-\frac{\partial f_p^0}{\partial E} \right) d\mathbf{k} \int_{-\infty}^{\phi} \mathbf{v} K(\phi, \phi') d\phi' \quad (4.22)$$

and

$$\boldsymbol{\Lambda}_p = -\frac{e}{\omega} \int \left(\frac{\mathbf{q} \cdot \mathbf{v}}{\omega_{ep}} \right) (\mathbf{q} \cdot \mathbf{V}_p) \left(-\frac{\partial f_p^0}{\partial E} \right) \times \int_{-\infty}^{\phi} (\mathbf{q} \cdot \mathbf{v}) \left(\frac{\mathbf{q} \cdot \mathbf{V}_p}{e\omega} \right) K(\phi, \phi') d\phi'. \quad (4.23)$$

D. Solution of A^{\pm}

Having obtained $\boldsymbol{\varepsilon}$, \mathbf{F}_e , and \mathbf{F}_D , we can now derive the expression for A^{\pm} . From Eqs. (4.2), (4.16), (4.19), and (4.21), A^{\pm} can be written as

$$A^{\pm} = \pm iM\Omega_c + \left\{ Z e + \frac{m}{2Ne} \left[-i\sigma_0\beta \left(\frac{1}{\tau_h} - \frac{1}{\tau_e} \right) + \left(\frac{1}{\tau_h} + \frac{1}{\tau_e} \right) (\sigma_h^{\pm} + \sigma_e^{\pm}) \right] + \frac{1}{N} (D_h'^{\pm} - D_e'^{\pm}) \right\} \times \left\{ ZNe + \frac{m}{e\tau_h} \sigma_h^{\pm} - \frac{m}{e\tau_e} \sigma_e^{\pm} + D_e^{\pm} - D_h^{\pm} \right\} / (\sigma_e^{\pm} + \sigma_h^{\pm} + i\sigma_0\beta) - \frac{1}{N} \left(\frac{m}{e\tau_e} D_e'^{\pm} + \frac{m}{e\tau_h} D_h'^{\pm} + \boldsymbol{\Lambda}_e^{\pm} + \boldsymbol{\Lambda}_h^{\pm} \right) + \frac{m}{N} \left[\frac{N_e}{\tau_e} + \frac{N_h}{\tau_h} + \frac{ZN}{2} \left(\frac{1}{\tau_h} - \frac{1}{\tau_e} \right) - \frac{1}{2e} \left(\frac{1}{\tau_h} + \frac{1}{\tau_e} \right) \left(\frac{m}{e\tau_h} \sigma_h^{\pm} + \frac{m}{e\tau_e} \sigma_e^{\pm} - D_h^{\pm} - D_e^{\pm} \right) \right], \quad (4.24)$$

where $\Omega_c = ZeH/Mc$ is the ionic cyclotron frequency. We see that A^{\pm} is a complicated function of σ^{\pm} , D^{\pm} , D'^{\pm} , and $\boldsymbol{\Lambda}^{\pm}$, which in turn depends on H . The H dependence of these four quantities will be discussed in the next section.

E. Conductivity σ^{\pm} and Deformation D^{\pm} , D'^{\pm} , and $\boldsymbol{\Lambda}^{\pm}$

1. Conductivity

Because of the symmetry conditions imposed by using circularly polarized sound, it is only necessary to consider the xx and yx components of the conductivity and deformation tensors. Following Stolz,¹³ the conductivity tensor as defined by Eq. (4.14) can be rewritten in circular coordinates as

$$\sigma^{\pm} = \sigma_{xx} \pm i\sigma_{yx} = \frac{e^2}{4\pi^3 \hbar^2} \int_{-k_{zF}}^{k_{zF}} \frac{m_c}{\omega_c} dk_z \times \int_0^{2\pi} (v_x \pm iv_y) d\phi \int_{-\infty}^{\phi} v_x' K(\phi, \phi') d\phi', \quad (4.25)$$

where $K(\phi, \phi')$ is defined by Eq. (4.12) and k_{zF} is the maximum extension of the Fermi surface along k_z .

The velocity can be expanded⁴⁴ in a Fourier series in ϕ as

$$\sigma^{\pm} = \frac{e^2}{8\pi^3 \hbar^2} \int_0^{k_{zF}} m_c \sum_l \left[\frac{A_{l+1}^2}{1 + i\omega_c \tau (X - \omega/\omega_c \mp g(l+1))} + \frac{A_{l+1}^2}{1 + i\omega_c \tau (-X - \omega/\omega_c \mp g(l+1))} + \frac{A_{l+3}^2}{1 + i\omega_c \tau (X - \omega/\omega_c \pm g(l+3))} + \frac{A_{l+3}^2}{1 + i\omega_c \tau (-X - \omega/\omega_c \pm g(l+3))} \right] dk_z, \quad (4.27)$$

$$v_x = \sum_l A_{l+1} \cos[g(l+1)\phi] + \sum_l A_{l+3} \cos[g(l+3)\phi],$$

$$v_y = \sum_l A_{l+1} \sin[g(l+1)\phi] - \sum_l A_{l+3} \sin[g(l+3)\phi],$$

$$v_z = \sum_r B_r \cos(r\phi), \quad (4.26)$$

where $B_0 = \bar{v}_z$ and r and l denote the harmonics of the Fourier expansion of v . For a Fermi surface centered at Γ in the Brillouin zone of s -fold rotational symmetry about the k_z axis, $l=0, 4, 8$ and $r=0, s, 2s, \dots$, where $s=3, 4$, and 6 . For Fermi surfaces not centered at Γ , the velocity expansion becomes more complicated. Elliptical Fermi surfaces, however, are simple to treat and are dealt with in Appendix A. In the following discussion we treat only those surfaces centered on Γ . The quantity $g=+1$ for holes, which move clockwise through their orbit in our coordinate system, and $g=-1$ for electrons which move counterclockwise.

To demonstrate the magnetic field dependence of the conductivity under the conditions of Doppler-shifted cyclotron resonance, let us first assume that v_z is independent of ϕ . Thus, we neglect the effects of geometric resonance. As shown in detail in Appendix A, Eqs. (4.25) and (4.26) then yield

⁴⁴ H. Aubauer (private communication and to be published).

where $X = q\bar{v}_z/\omega_c$. Using the relationship⁴⁵

$$m_e \bar{v}_z = \frac{\hbar}{2\pi} \frac{\partial \mathcal{Q}}{\partial k_z}, \quad (4.28)$$

we can write X as

$$X = \frac{q\hbar}{2\pi e c H} \frac{1}{\partial k_z} \frac{\partial \mathcal{Q}}{\partial k_z}. \quad (4.29)$$

The quantity \mathcal{Q} is the cross-sectional area of the Fermi surface in a plane perpendicular to H . If $\partial \mathcal{Q}/\partial k_z$ is constant over an appreciable range of k_z , then at certain magnetic fields H_I , there will be peaks in $\text{Re}\sigma^\pm$. The fields H_I are given by the relationship

$$|X| = \left| \frac{q\hbar}{2\pi e c H_I} \frac{1}{\left(\frac{\partial \mathcal{Q}}{\partial k_z}\right)_{\text{const}}} \right| = I \quad (4.30)$$

if we assume that the Fourier coefficients A_{l+1} and A_{l+3} are independent of k_z and that the term ω/ω_c in Eq. (4.27), which arises from the finite velocity of sound, can be ignored. Here $(\partial \mathcal{Q}/\partial k_z)_{\text{const}}$ represents that value of $\partial \mathcal{Q}/\partial k_z$ which is constant over an appreciable range of k_z . In the present case where $v_z = \bar{v}_z$, $I = 1, 3, 5 \dots$.

The strength of these peaks will depend on the magnitude of the corresponding Fourier coefficients, and also on $\omega_c \tau$. For those Fermi surfaces having full rotational symmetry about k_z , $A_3 = 0$, $A_5 = 0, \dots$, only the H_I peak will appear in $\text{Re}\sigma^\pm$. These peaks in $\text{Re}\sigma^\pm$ are known as Doppler-shifted cyclotron resonance peaks.

Equation (4.30) shows that a plot of peak number (1, 3, 5, ...) versus $1/H_I$ will yield a straight line whose slope is proportional to $(\partial \mathcal{Q}/\partial k_z)_{\text{const}}$ unless the Fourier coefficients are strongly k_z -dependent. A strong k_z dependence of the Fourier coefficients causes the peaks in $\text{Re}\sigma^\pm$ to shift from H_I , and Eq. (4.30) will no longer be valid in determining peak positions.

The line shape of these peaks will depend on the higher derivatives of \mathcal{Q} with respect to k_z and also on τ . The peaks will generally be asymmetrical in shape although shorter relaxation times will tend to smooth out the peaks and decrease the asymmetry.

In some cases $\partial \mathcal{Q}/\partial k_z$ will not be constant (or nearly constant) over any part of the Fermi surface. In this case there will not be any peaks in $\text{Re}\sigma^\pm$. An edge in $\text{Re}\sigma^\pm$ will appear at H_A^I whenever

$$|X| = \left| \frac{q\hbar}{2\pi e c H_A^I} \frac{1}{\left(\frac{\partial \mathcal{Q}}{\partial k_z}\right)_{\text{max}}} \right| = I, \quad (4.31)$$

where $(\partial \mathcal{Q}/\partial k_z)_{\text{max}}$ is the maximum value of $\partial \mathcal{Q}/\partial k_z$. This edge will occur for any Fermi surface whether it gives rise to peaks in $\text{Re}\sigma^\pm$ or not. An example is an ellipsoid whose principal axis is tilted with respect to H and where $\partial \mathcal{Q}/\partial k_z = ck_z$. Then there will be no peaks in $\text{Re}\sigma^\pm$ but a series of edges at H_A^I , where H_A^I is

determined by

$$\left| \frac{q\hbar}{2\pi e c H_A^I} ck_{zF} \right| = I.$$

For the ellipsoid, the shape of the edge depends on the principal radii of curvature and relaxation time as discussed by Kjeldaa.

In the previous discussion we have ignored the ω/ω_c term of Eq. (4.27). This term is related to v_s/v_F and allows one to distinguish between electrons and holes in σ^\pm . If we rewrite Eq. (4.30) taking into account the ω/ω_c term in Eq. (4.27), we get

$$\begin{aligned} & \left| \frac{q\hbar}{2\pi e c H_J} \frac{1}{\left(\frac{\partial \mathcal{Q}}{\partial k_z}\right)_{\text{const}}} \right| \mp g\omega/\omega_c = J \\ \text{and} & \left| \frac{q\hbar}{2\pi e c H_{J'}} \frac{1}{\left(\frac{\partial \mathcal{Q}}{\partial k_z}\right)_{\text{const}}} \right| \pm g\omega/\omega_c = J', \end{aligned} \quad (4.32)$$

where $J = 1, 5, 9 \dots$, and $J' = 3, 7, 11 \dots$. For a hole surface ($g = +1$) and a right-handed wave (+), the H_J peaks are shifted to lower fields and the $H_{J'}$ peaks to higher fields with respect to the corresponding peaks at H_I . The opposite occurs for left-handed waves. This is in agreement with the conditions classifying resonances as Type A or B, as stated in Eqs. (1.3) and (1.4).

The symmetry relations $\text{Re}\sigma^\pm(H) = \text{Re}\sigma^\pm(-H)$ and $\text{Im}\sigma^\pm(H) = -\text{Im}\sigma^\pm(-H)$ follow from Eq. (4.27).

By assuming that $v_z = \bar{v}_z$, σ^\pm takes on the simple form given in Eq. (4.27). However, v_z may be a function of ϕ . When v_z is expanded in a Fourier series [(Eq. (4.26))] and inserted into Eq. (4.25), $K(\phi, \phi')$ after integration over ϕ'' , becomes

$$K(\phi, \phi') = \exp \left[i(X - \omega/\omega_c)(\phi' - \phi) + i \left(\sum_r c_r \sin(r\phi') - c_r \sin(r\phi) \right) + \frac{\phi' - \phi}{\omega_c \tau} \right].$$

The quantities $c_r = qB_r/\omega_c \tau$, $c_0 = 0$, and $X = q\bar{v}_z/\omega_c$. The term $K(\phi, \phi')$ will introduce Bessel functions into the integrand of σ^\pm , since $\exp[iW \sin \phi] = \sum_m J_m(W) e^{im\phi}$, where J_m is the m th-order integer Bessel function and $m = 0, \pm 1, \pm 2 \dots$. Equation (4.25) can be solved using the Fourier expansions of v_x and v_y as before (see Appendix A). The exact expression of σ^\pm is a complicated expression consisting of summations over $l, l', r, m_1, m_1', \dots, m_r, m_r'$, and m_r' . A typical term in the summation is

$$\begin{aligned} \sigma^\pm(l, l', r, m_1, m_1', \dots, m_r, m_r') &= \frac{e^2}{8\pi^3 \hbar^2} \int_0^{k_{zF}} m_c dk_z \\ &\times \left[\frac{A_{l+1} A_{l'+1} \prod_r J_{m_r}(c_r) J_{m_r'}(c_r)}{1 + i\omega_c \tau (X - \omega/\omega_c \mp g(l+1) - \sum_r m_r r)} \right]. \end{aligned} \quad (4.33)$$

⁴⁵ W. Harrison, Phys. Rev. 118, 1190 (1960).

TABLE IV. Values of I for which peaks or edges may appear in Λ^\pm , D^\pm , D'^\pm , and σ^\pm at H_I or H_A^I , respectively (see text).

Tensor quantity	Condition (ϕ dependence of v_z and V_{zx})	Fermi surfaces centered at Γ			Fermi surfaces not centered at Γ (elliptical pieces) 3, 4, or 6-fold rotational symmetry about k_z
		3-fold rotational symmetry about k_z	4-fold rotational symmetry about k_z	6-fold rotational symmetry about k_z	
σ^\pm	$v_z = \bar{v}_z$	$I = 1, 3, 5 \dots$	$I = 1, 3, 5 \dots$	$I = 1, 3, 5 \dots$	$I = 1$ only
	$v_z = f(\phi)$	$I = 1, 2, 3 \dots$	$I = 1, 3, 5 \dots$	$I = 1, 3, 5 \dots$	$I = 1, 2, 3 \dots$
D^\pm	$v_z = \bar{v}_z, V_{zx} = \text{const}$	$D^\pm = 0$	$D^\pm = 0$	$D^\pm = 0$	$D^\pm = 0$
	$v_z = \bar{v}_z, V_{zx} = f'(\phi)$	$I = 3, 9, 15$	$D^\pm = 0$	$D^\pm = 0$	$I = 1$ only
	$v_z = f(\phi), V_{zx} = \text{const}$	$I = 1, 2, 3 \dots$	$D^\pm = 0$	$D^\pm = 0$	$I = 1, 2, 3 \dots$
	$v_z = f(\phi), V_{zx} = f'(\phi)$	$I = 1, 2, 3 \dots$	$D^\pm = 0$	$D^\pm = 0$	$I = 1, 2, 3 \dots$
D'^\pm	$v_z = \bar{v}_z, V_{zx} = \text{const}$	$D'^\pm = 0$	$D'^\pm = 0$	$D'^\pm = 0$	$D'^\pm = 0$
	$v_z = \bar{v}_z, V_{zx} = f'(\phi)$	$I = 3, 9, 15 \dots$	$D'^\pm = 0$	$D'^\pm = 0$	$I = 1$ only
	$v_z = f(\phi), V_{zx} = \text{const}$	$I = 1, 2, 3 \dots$	$D'^\pm = 0$	$D'^\pm = 0$	$I = 1, 2, 3 \dots$
	$v_z = f(\phi), V_{zx} = f'(\phi)$	$I = 1, 2, 3 \dots$	$D'^\pm = 0$	$D'^\pm = 0$	$I = 1, 2, 3 \dots$
Λ^\pm	$v_z = \bar{v}_z, V_{zx} = \text{const}$	$\Lambda^\pm = \text{const}$	$\Lambda^\pm = \text{const}$	$\Lambda^\pm = \text{const}$	$\Lambda^\pm = \text{const}$
	$v_z = \bar{v}_z, V_{zx} = f'(\phi)$	$I = 3, 6, 9 \dots$	$I = 4, 8, 12 \dots$	$I = 6, 12, 18 \dots$	$I = 1, 2, 3 \dots$
	$v_z = f(\phi), V_{zx} = \text{const}$	$I = 3, 6, 9 \dots$	$I = 4, 8, 12 \dots$	$I = 6, 12, 18 \dots$	$I = 1, 2, 3 \dots$
	$v_z = f(\phi), V_{zx} = f'(\phi)$	$I = 3, 6, 9 \dots$	$I = 4, 8, 12 \dots$	$I = 6, 12, 18 \dots$	$I = 1, 2, 3 \dots$

If the k_z dependence of the Bessel functions and Fourier coefficients in Eq. (4.33) can be neglected, then for 4-fold rotationally symmetric Fermi surfaces centered on Γ , peaks in $\text{Re}\sigma^\pm$ will again occur at H_1, H_3, H_5, \dots as in the case of $v_z = \bar{v}_z$, because $r = 0, 4, 8, \dots$. However, for other symmetries additional peaks may be introduced when v_z is a function of ϕ , as seen in Table IV. If the Bessel functions are k_z -dependent, then the peaks arising at H_I , will be shifted in addition to any peak shift caused by the Fourier coefficients.

In addition to possibly shifting the Doppler-shifted cyclotron resonance peaks in $\text{Re}\sigma^\pm$, the Bessel functions may themselves cause oscillations in $\text{Re}\sigma^\pm$, since at low magnetic fields the Bessel functions oscillate sinusoidally. These oscillations are known as geometric resonance. Since c_r does not depend upon the polarization of the sound wave, there will be no difference in the effects of right- or left-handed waves on geometric resonance. There will also be no difference in the geometric resonance between longitudinal and shear waves, since c_r is the same in both cases. This is confirmed by the agreement between our results and those of Beckman *et al.* in Sb.

The denominators in the integrand of σ^\pm , which give rise to Doppler-shifted cyclotron resonance, also cause rapid variations in σ^\pm at low magnetic fields, as discussed earlier, so that Doppler-shifted and geometric resonances may simultaneously appear. In some cases the denominator may remain constant as a function of H and k_z . In this case only the Bessel functions cause σ^\pm to vary. In particular, this happens when $\bar{v}_z = 0$, and then $X = 0$. An example of this is a cylinder whose axis is tilted with respect to H and where $\bar{v}_z = 0$ over all k_z . Then $c_r = qB_r/\omega\mathcal{G}$ is finite and only geometric resonance will be observed.

2. Deformation Terms $D^\pm, D'^\pm, \Lambda^\pm$

The deformation tensors given by Eqs. (4.15), (4.22), and (4.23) can be written in circular coordinates analogous to the conductivity given by Eq. (4.25). In evaluating these deformation terms, the ϕ dependence of the components of the deformation potential V_{zx} and V_{zy} must be taken into account. The deformation potential can be expanded in a Fourier series as

$$V_{zx} = \sum_r E_r \cos r\phi, \quad (4.34)$$

$$V_{zy} = \sum_r E_r' \sin r\phi,$$

where $E_r = E_r'$ and $r = 0, s, 2s, \dots$ for s -fold rotationally symmetric surfaces centered on Γ , and $E_r \neq E_r'$ and $r = 1, 2, 3, \dots$ for elliptical surfaces not centered at Γ . Using Eqs. (4.26) and (4.34), the deformation terms can be evaluated and result in an expression similar to σ^\pm .

The final expressions for D^\pm, D'^\pm , and Λ^\pm show that Doppler-shifted cyclotron resonance and geometric resonance occur. The allowed peaks at H_I and edges at H_A^I are given in Table IV. The geometric resonances occurring in D^\pm, D'^\pm , and Λ^\pm are the same as those occurring in σ^\pm since the function $K(\phi, \phi')$ appears in the expressions of all four quantities.

The $\text{Re}D^\pm(H) = \text{Re}D^\mp(-H)$, $\text{Im}D^\pm(H) = -\text{Im}D^\mp \times (-H)$, etc., can be shown to hold as in the case of σ^\pm .

The quantity Λ^\pm is proportional to V_{zx}^2 , and since V_{zx} is zero for spherical Fermi surfaces⁴⁶ and small for nearly-free-electron metals, one expects Λ^\pm to be very small for most metals. The total magnitude of the shear-deformation contribution to the attenuation can be

⁴⁶J. M. Ziman, *Electrons and Phonons* (Clarendon Press, Oxford, England, 1963), p. 216.

estimated for certain metals from measurements of the temperature dependence of the attenuation in the normal and superconducting state. From measurements on the attenuation of shear waves in Al by David *et al.*,⁴⁷ Liebowitz⁴⁸ has shown that 10% of the total attenuation for shear waves propagated along the [110] direction is due to deformation effects. In Sn, Liebowitz⁴⁹ has found the deformation contribution to be about 30% of the total attenuation for shear waves propagating along the [001] direction.

F. Discussion of A^\pm

It is possible to draw some general conclusions regarding A^\pm from the properties exhibited by σ^\pm , D^\pm , D'^\pm , and Λ^\pm . From the symmetry properties of these quantities we can show that

$$\text{Re}[A^\pm(H) - A^\pm(0)] = \text{Re}[A^\mp(-H) - A^\mp(0)]$$

and

$$\text{Im}(A^\pm(H) - A^\pm(0)) = -\text{Im}(A^\mp(-H) - A^\mp(0)).$$

This is in agreement with the Kjeldaas theory and confirms Eq. (3.4).

We have seen that the conductivity and deformation terms give rise to geometric resonances, which vary sinusoidally with respect to $1/H$, and Doppler-shifted cyclotron resonance which causes asymmetric peaks nearly periodic in $1/H$. The sinusoidal oscillations coming from the geometric resonances will suffer only amplitude and phase change, when combined in Eq. (4.24) to form A^\pm . Thus, by measuring the period of the oscillations in $1/H$ of α^\pm , the amplitude of v_z as a function of ϕ can be determined.

It is possible that the Doppler-shifted cyclotron resonance peaks may also be periodic in $1/H$, in which case one can also analyze the period as determined from α^\pm , and obtain the value of $(\partial\alpha/\partial k_z)_{\text{const}}$. This assumes that the peaks in $\text{Re}\sigma^\pm$, $\text{Re}D^\pm$, $\text{Re}D'^\pm$, and $\text{Re}\Lambda^\pm$ all occur at the same H_I . In general, this periodicity in $1/H$ will not be present because of the Fourier coefficients or the Bessel functions, or it may be extremely difficult to identify peak positions in H because of the

asymmetry of the peaks. Sometimes only the first peak in a family will appear (e.g., tin) in α^\pm . In any of the above cases the only way to relate these peaks (or peak) to $(\partial\alpha/\partial k_z)_{\text{const}}$ is through Eq. (4.24). Under certain conditions it is possible to relate a single peak in α^\pm to $(\partial\alpha/\partial k_z)_{\text{const}}$ without having to explicitly evaluate Eq. (4.24), as will be shown later.

The symmetry of the Fermi surface plays an important role in the form of Eq. (4.24), through the ϕ dependence of v_r and V_{zz} . For example, a Fermi surface centered on Γ with 4- or 6-fold rotational symmetry about k_z would cause A^\pm to depend upon σ^\pm and Λ^\pm only. If v_z and V_{zz} are independent of ϕ , then A^\pm depends only on σ^\pm , since Λ^\pm would be independent of H as seen in Table IV.

The way in which the conductivity and deformation terms are combined to form A^\pm depends upon the constants in Eq. (4.24) (e.g., N , N_e , N_h , etc.). In this relationship, the number of electrons and holes present in the metal play a very important role, giving us three cases to consider: (1) both electrons and holes present, but $N_e \neq N_h$; (2) electrons and holes present, and $N_e = N_h$; (3) only electrons or holes present.

Case 1. There can be no simplification of Eq. (4.24). It should be noted that A^\pm is proportional to D^\pm , D'^\pm , Λ^\pm , σ^\pm , and the cross products $D^\pm D'^\pm$, $\sigma^\pm D'^\pm$, etc., while it is inversely proportional to σ^\pm . Thus, the field dependence of A^\pm will depend upon the relative strength between the deformation and conductivity terms, which in turn depends upon the Fermi surface in question. Unfortunately, in this case the deformation and conductivity terms must be evaluated before they can be compared with experiment.

Case 2. When $N_e = N_h$, then $Z=0$ and Eq. (4.24) can be simplified somewhat. A^\pm is proportional to such terms as σ^\pm , D^\pm , D'^\pm , Λ^\pm , $\sigma^\pm/(\sigma_e^\pm + \sigma_h^\pm)$, $\sigma_e^\pm \sigma_h^\pm/(\sigma_e^\pm + \sigma_h^\pm)$, $\sigma^\pm D^\pm/(\sigma_e^\pm + \sigma_h^\pm)$, etc., if $\sigma_0\beta \ll \sigma^\pm$ is neglected. For those Fermi surfaces where σ^\pm , D^\pm , and D'^\pm all have the same H dependence, we would expect the H dependence of A^\pm to be nearly proportional to the conductivity and deformation terms.

Case 3. If only electrons or holes are present, then Eq. (4.24) reduces to

$$A^\pm = \frac{(Ze - ig(m\sigma_0/N_e\tau_p)\beta) + (g/N)D_p'^\pm)(ZNe + g(m\sigma_p^\pm/\epsilon\tau_p) - gD_p^\pm)}{\sigma_p^\pm + i\beta\sigma_0} - \frac{1}{N} \left(\frac{mD'^\pm}{\epsilon\tau_p} + \Lambda_p \right) \pm i\Omega_c M. \quad (4.35)$$

Equation (4.35) shows that a peak in $\text{Re}\sigma^\pm$ will result in a dip in $\text{Re}A^\pm$, while a peak in $\text{Re}D^\pm$, $\text{Re}D'^\pm$, and $\text{Re}\Lambda^\pm$ will give a peak in $\text{Re}A^\pm$. The resulting A^\pm dependence will depend upon the relative strength of the various terms.

⁴⁷ R. David, H. R. Van der Laan, and N. J. Poulis, *Physica* **29**, 357 (1963).

⁴⁸ J. R. Liebowitz, *Phys. Rev.* **136**, A22 (1964).

⁴⁹ J. R. Liebowitz, *Phys. Rev.* **136**, A84 (1964).

For a spherical Fermi surface, Eq. (4.35) reduces to

$$A^\pm = \frac{(Ze - ig(m\sigma_0/N_e\tau_p)\beta)(ZNe + g(m\sigma_p^\pm/\epsilon\tau_p))}{\sigma_p^\pm + i\beta\sigma_0} \pm iM\Omega_c \quad (4.36)$$

since D^\pm , D'^\pm , and Λ^\pm are then zero. Here A^\pm is proportional to $1/\sigma_p^\pm$ and a peak in $\text{Re}\sigma^\pm$ will result in a dip in $\text{Re}A^\pm$.

For a free-electron spherical Fermi surface, Eq. (4.36) can be shown to yield the Kjeldaas result.

V. DISCUSSION

We have seen how the compensation ($N_e - N_h$) affects the relationship between A^\pm and σ^\pm , D^\pm , D'^\pm , and Λ^\pm , and the following discussion treats our results, and those of others, according to the compensation.

A. Complete Compensation $N_e = N_h$

Metals which have an even number of electrons per unit cell, such as antimony with ten and tin with eight electrons per unit cell, are compensated.

1. Antimony

The Fermi surface of Sb is composed of electron and hole pieces which are nearly ellipsoidal. Windmiller³⁵ and Falicov and Lin³⁶ have shown that there are six hole surfaces with mirror symmetry, whose principal axis is tilted at 53° away from the trigonal axis, and 3 electron surfaces located at the point L of the Brillouin zone, whose principal axis is tilted at 88° from the trigonal axis. Each of the hole surfaces can be characterized by an ellipsoid with the following energy equation:

$$\frac{2mE_F}{\hbar^2} = \alpha_{11}k_x^2 + \alpha_{22}k_y^2 + \alpha_{33}k_z^2 + \alpha_{23}k_yk_z, \quad (5.1)$$

written in the coordinate system of the crystal centered

$$\sigma^\pm = \left(\frac{3}{16} \frac{e^2}{\hbar^2 \pi^3} m_c \left(\frac{2E_F}{m} \right)^{1/2} \right) J_1^2 \left(\frac{q\alpha_{23} \left[\frac{2mE_F}{\alpha_{22}} \right]^{1/2}}{m\omega_c} \right) (\alpha_{11} + \alpha_{22}) \Delta k_z / (1 + i\omega\tau), \quad (5.4)$$

where J_1 is the first-order Bessel function, and $\omega_c = (eH/mc)(\alpha_{11}\alpha_{22})^{1/2}$. Since we are only considering the $k_z \approx 0$ orbit ($\bar{v}_z = 0$), integration over k_z was not performed. The quantity Δk_z is the width of the band of electrons at $k_z \approx 0$ participating in geometric resonance. There are other terms in Eq. (5.4) but they have factors of $\omega_c\tau$ in the denominator, and since $\omega_c\tau \approx 100$, we have neglected them.

The quantity $J_1(W) \approx \cos(W - \frac{3}{4}\pi)$ for $W > 3$ and hence $J_1^2(W)$ becomes a maximum at $W = \frac{3}{4}\pi, (7/4)\pi, \dots$. Thus, the Bessel function is periodic in $1/H$ with a period of

$$\Delta(1/H) = - \frac{\lambda e}{2c} \left(\frac{\alpha_{11}}{2mE_F} \right)^{1/2} \frac{\alpha_{22}}{\alpha_{23}}, \quad (5.5)$$

which is identical to the condition derived by Beckman *et al.*⁸ and Quinn.¹⁴ Using the values $\alpha_{11} = 0.965 \times 10^{14} E_F$, $\alpha_{22} = 0.426 \times 10^{14} E_F$, $\alpha_{33} = 0.588 \times 10^{14} E_F$, and $\alpha_{23} = 0.576 \times 10^{14} E_F$, as derived from Windmiller's data, and $E_F = 18.6 \times 10^{-14}$ erg from Schoenberg,³⁸ in Eq. (5.5) gives $\Delta(1/H) = 0.00472 \text{ G}^{-1}$, which should be compared to our experimental value of $\Delta(1/H) = 0.00442 \pm 0.0002 \text{ G}^{-1}$.

on the ellipsoid. The velocity of the holes can be written as

$$\mathbf{v} = (\hbar/m)\boldsymbol{\alpha} \cdot \mathbf{k}. \quad (5.2)$$

Each of the electron surfaces can also be characterized by an ellipsoid having the energy equation

$$\frac{2mE_F}{\hbar^2} = \beta_1 k_x^2 + \beta_2 k_y^2 + \beta_3 k_z^2. \quad (5.3)$$

For simplicity we have neglected the 2° deviation between the principal axis of the electron surface and the binary-bisectrix plane of the crystal.

For the hole surface, v_z will vary through the orbit due to the 53° tilt from the trigonal giving rise to geometric resonance. From Table IV we see that Doppler-shifted cyclotron edges will occur at H_A^I , where $I = 1, 2, 3, \dots$, in $\text{Re}\sigma^\pm$, $\text{Re}D^\pm$, $\text{Re}D'^\pm$, and $\text{Re}\Lambda^\pm$. The velocity v_z on the electron surface will be constant through the orbit and will give no geometric resonances. From Table IV edges will occur at H_A^1 in $\text{Re}\sigma^\pm$, $\text{Re}D^\pm$, and $\text{Re}D'^\pm$ and at $H_A^1, H_A^2, H_A^3, \dots$ in $\text{Re}\Lambda^\pm$ for the electron surface. Those results apply to the most general case where V_{zx} and V_{zy} are functions of \mathbf{k} .

Let us first consider the geometric resonances arising from the hole surface. By solving the equation of motion for holes in the presence of a magnetic field, the velocities v_x , v_y , and v_z can be determined by using Eqs. (5.1) and (5.2) as seen in Appendix B. Using these velocities in Eq. (4.25) yields the solution (see Appendix A) for the $k_z = 0$ orbit

To determine where the Doppler-shifted cyclotron resonance edges occur, we need to compute $(\partial\alpha/\partial k_z)_{\text{max}}$ as seen from Eq. (4.31). From the value of X as determined in Appendix B, we find that $(\partial\alpha/\partial k_z)_{\text{max}} = 2\pi(\alpha_{33} - \alpha_{23}/\alpha_{22}) k_{zF}$ for the hole surfaces, and $(\partial\alpha/\partial k_z)_{\text{max}} = 2\pi\beta_3 k_{zF}$ for the electron surfaces. For the hole surfaces $k_{zF} = 5.36 \times 10^6 \text{ cm}^{-1}$, and for the electron surfaces $k_{zF} = 8.38 \times 10^6 \text{ cm}^{-1}$. Using the previous values of α_{11} , α_{22} , α_{33} , α_{23} , and E_F , Eq. (5.30) gives a value of H_A^I as

$$H_A^I = 280/I \text{ G}$$

for holes. Since $I = 1, 2, 3, \dots$ we would expect a series of edges periodic in $1/H$ to appear in the attenuation because α^\pm is proportional to $\text{Re}(\sigma^\pm + D^\pm + D'^\pm + \Lambda^\pm)$ in a compensated metal. Similarly by using the value of $\beta_3 = 0.236 \times 10^{14} E_F$ we get

$$H_A^I = 350/I \text{ G}$$

for electrons. The fact that there is no experimental evidence of these edges, as seen in Fig. 11, implies that Doppler-shifted cyclotron resonance is weak in this case.

2. Tin

The detailed structure of the Fermi surface of Sn indicates a complicated topological figure which makes any computation of σ^\pm , D^\pm , D'^\pm , and Λ^\pm nearly impossible. However, for Sn, which has 4-fold rotational symmetry about H , α is proportional to σ^\pm , D^\pm , D'^\pm , and Λ^\pm since σ^\pm , D^\pm , and D'^\pm all have the same H dependence (see Table IV). This holds for the surfaces centered on Γ and not on Γ .

Figure 6 shows that certain peaks (1, 10, 11, 19, 24, and 32) are Doppler-shifted cyclotron resonance peaks because of their sharpness, asymmetrical character, and difference in H for the (+) and (-) wave. They are probably H_1 peaks because of their strength. If so, and if we assume that the position of H_1 is unaffected by the Fourier coefficients and Bessel functions in the integrands of σ^\pm , D^\pm , D'^\pm , and Λ^\pm , then we can state the following condition for the maximum in $\text{Re}A^\pm$:

$$\left| \frac{q_c}{e} \frac{1}{H_1^\pm} (m_c \bar{v}_z)_{\text{const}} \right| \mp \omega/\omega_c = 1, \quad (5.6)$$

which follows from Eqs. (4.28) and (4.32). This means that if the product $m_c \bar{v}_z$ is constant over an appreciable range of the Fermi surface along k_z a peak will occur at H_1^\pm in $\text{Re}A^\pm$. By taking the sum and difference of the + and - parts of Eq. (5.6), we get

$$\frac{m_c}{m} = \frac{e}{2m_c\omega} |H_1^+ - H_1^-| \quad (5.7)$$

and

$$|\bar{v}_z| = v_s \left| \frac{H^+ + H^-}{H^+ - H^-} \right|. \quad (5.8)$$

Here m_c and \bar{v}_z are the cyclotron mass and average velocity along z belonging to that part of the Fermi surface giving rise to the peak at H_1^\pm . Applying Eqs. (5.7) and (5.8) to peak number 10 (the strongest peak) in Fig. 4 gives

$$m_c/m = 0.64 \pm 0.03 \quad \text{and} \quad |\bar{v}_z| = (0.133 \pm 0.007) \times 10^8.$$

This peak arises from a slice of the Fermi surface where \bar{v}_z is much less than the Fermi velocity v_F .

The weak peaks in Fig. 4 (Nos. 5 through 9) are caused either by geometric resonance or by the higher harmonics of the Doppler-shifted cyclotron resonance peaks, but it is difficult to determine which one is responsible because of the many processes which occur simultaneously.

B. Zero Compensation

The metals which have zero compensation are the alkali metals and noble metals, in particular, copper. In this case A^\pm is given by Eq. (4.35) and is proportional to the deformation terms and inversely proportional to the conductivity. Copper has 4-fold

rotational symmetry about $[100]$ and is centered on Γ , so one would expect the first-order deformation terms D^\pm , and D'^\pm to vanish when $q \parallel [100]$. However, the necks introduce complications and these two terms are probably present.⁵⁰

By using the Fermi surface of copper as computed by Roaf,⁵¹ Gavanda and Boyd¹⁰ were able to predict that H_1 in σ^\pm should occur near 4 kG for $q \parallel [100]$. This peak comes from the region of the Fermi surface where the necks join the belly. They then compared this peak directly with their measured attenuation peak at 4.3 kG. This agreement is surprising since it implies that A^\pm is proportional to σ^\pm instead of $1/\sigma^\pm$. However, A^\pm is proportional to D^\pm , D'^\pm , and Λ^\pm , and in general all these terms will give rise to a peak at H_1 . It is probable that the deformation terms are large since the region where the necks join the belly in copper is extremely sensitive to any strains induced by the acoustic wave. Thus, one expects that $\text{Re}D^\pm$ and especially $\text{Re}\Lambda^\pm$ to dominate the attenuation.

C. Incomplete Compensation $N_e \neq N_h$

Incomplete compensation occurs in polyvalent metals having an odd number of electrons per unit cell, such as Al.

In a preliminary calculation, Aubauer has obtained σ^\pm for the second zone holes in Al using a nearly-free-electron model. He included the Fourier coefficients of the velocity expansion in his calculation but assumed $v_z = \bar{v}_z$. For the $\text{Re}\sigma^\pm$ he found a family of peaks periodic in $1/H_I$ having a period of $1.15 \times 10^{-4} \text{ G}^{-1}$ with the H_1 peak occurring at 9 kG. By calculating $\text{Re}(1/\sigma^\pm)$, he also found a family of peaks periodic in $1/H_I$ having a period of $1.15 \times 10^{-4} \text{ G}^{-1}$ as before, but now the H_1 peak occurred at 3.9 kG. The H dependence of $\text{Re}(1/\sigma^\pm)$ resembles Fig. 7 and $\text{Im}(1/\sigma^\pm)$ resembles Fig. 10 very closely except for the exact peak positions and periodicity. This suggests that A^\pm is nearly proportional to $1/\sigma^\pm$ in Al. The discrepancy between the observed and calculated periodicities might be resolved by using a more accurate model for the Fermi surface of Al.⁵² A more complete calculation including the effects of the Bessel functions is now in progress.

It is surprising that Jones,⁵ by assuming that the attenuation was proportional to the conductivity,⁵³

⁵⁰ If one treats the necks in the Fermi surface of Cu as cylinders centered on L , they will have the same properties as ellipsoids at L with regard to which peaks are allowed by symmetry (see Table IV).

⁵¹ D. J. Roaf, Phil. Trans. Roy. Soc. London A255, 135 (1962).

⁵² Phonon renormalization corrections will enter both \bar{v}_z and ω_c . If the two corrections are identical, they will of course cancel out in the determination of the peak position leaving only the geometric quantity $\partial G/\partial K_z$. If not, there could be an effect of phonon renormalization on the period. However, it seems unlikely that it is able to account for the discrepancy of a factor of 1.5; an explicit theoretical investigation of this problem would be of value. M. H. Cohen (private communication).

⁵³ Jones actually did not assume that α_{zz} was proportional to σ_{zz} . He derived a quantity from energy considerations which had the same form as σ_{zz} and set this proportional to α_{zz} .

accounted for his attenuation results as being due to the second zone hole surface in Al. He propagated longitudinal waves along the [100] axis of Al with $\mathbf{q} \parallel \mathbf{H}$ and found that the first peak in a family of peaks (periodic in $1/H$) occurred at 0.65 kG.

For longitudinal waves the substitution $A^\pm \rightarrow A_{zz}$, $\sigma^\pm \rightarrow \sigma_{zz}/1 - R_{zz}$, $D^\pm \rightarrow D_{zz}$, $D'^\pm \rightarrow D'_{zz}$ and $\Lambda^\pm \rightarrow \Lambda_{zz}$ can be made in Eq. (4.24). The diffusion term R_{zz} arises for longitudinal waves and is proportional to σ_{zz} . By assuming $A_{zz} \propto \sigma_{zz}$, Jones found, using the relations given in Eq. (4.30), that the peaks were caused by a region of the Fermi surface where $(\partial\alpha/\partial k_z)_{\text{const}} = 3.3k_0$, where $k_0 = 2\pi/a$ and a is the lattice spacing. From the free-electron Fermi surface of Al he found a region of constant slope in the second zone of about $3.3k_0$, from $k_z = 0.35k_0$ to $0.50k_0$. He suggested that this region of the Fermi surface was responsible for his peaks. This region is also responsible for the 9-kG peak in $\text{Re}\sigma^\pm$ calculated by Aubauer.

The fact that Jones can explain his data by assuming A_{zz} is proportional to σ_{zz} might be explained if D_{zz} , D'_{zz} , or Λ_{zz} become the dominant terms in A_{zz} , since $\text{Re}\sigma_{zz}$, $\text{Re}D_{zz}$, $\text{Re}D'_{zz}$, and $\text{Re}\Lambda_{zz}$ all have peaks at H_4, H_8, \dots . It is not unreasonable to expect that the longitudinal deformation terms may be large, because even in the case of a sphere where D^\pm, D'^\pm , and $\Lambda^\pm = 0$, D_{zz}, D'_{zz} , and Λ_{zz} are finite.

VI. CONCLUSION

The attenuation and dispersion of circularly polarized sound has been measured as a function of magnetic field oriented parallel to the sound propagation by using the method of split receiving transducers. This method eliminates any ambiguity in the measurement of the attenuation that might be caused by rotations of the plane of polarization of the sound wave. A further advantage of this method is that information can be obtained about the sign of the carriers contributing to the structure in the magnetoacoustic attenuation caused by Doppler-shifted cyclotron resonance.

There are two mechanisms responsible for the attenuation: Geometric resonance and Doppler-shifted cyclotron resonance. Geometric resonance appears in the attenuation as a damped sinusoidal oscillation periodic in $1/H$ and is independent of sound polarization. The period can be related to an orbit on the Fermi surface where the average velocity \bar{v}_z along H is nearly equal to zero and whose instantaneous velocity v_z is nonzero. Doppler-shifted cyclotron resonance appears in the attenuation as families of asymmetric peaks or absorption edges each of which is nearly periodic in $1/H$. This periodicity can be related to that section of the Fermi surface where $\partial\alpha/\partial k_z$ or $m_e\bar{v}_z$ is constant over a wide range of k_z .

When electrons and holes are present the observed structure in the attenuation, such as peak position or peak shape, cannot simply be related to the Fermi

surface. Instead, the expression for the attenuation depends in a complicated way on the components of the conductivity and deformation tensors, which in turn depend on the details of the Fermi surface. Such details include the k dependence of the Fermi velocity and the deformation potential over the entire Fermi surface.

The Fermi surface of Sb consists of ellipsoidal pieces which should give rise to Doppler-shifted cyclotron resonance edges. However, no edges were observed. Instead, a damped sinusoidal oscillation periodic in $1/H$ was seen and identified as geometric resonance. The observed period of $(0.44 \pm 0.02) \times 10^{-4} \text{ G}^{-1}$ agrees with the period $0.47 \times 10^{-4} \text{ G}^{-1}$ expected from the $k_z = 0$ orbit of the tilted hole surface of Sb.

Over thirty peaks in the attenuation for Sn could be identified, many as Doppler-shifted cyclotron resonance peaks. Unfortunately, because of the complicated Fermi surface of Sn, no relation between the peaks and the Fermi surface could be made.

For Al the measured attenuation peaks were nearly periodic in $1/H$ having a period of $(1.8 \pm 0.04) \times 10^{-4} \text{ G}^{-1}$ with the high-field peak occurring at 3.2 kG. By observing the relative peak shift of the right- and left-handed waves, it was established that these peaks were caused by the second Brillouin zone hole surface. By assuming that the attenuation is inversely proportional to the conductivity, the attenuation was calculated using the nearly-free-electron model for the second zone holes. It was found that the calculated attenuation has peaks which are periodic in $1/H$ having a period of $1.15 \times 10^{-4} \text{ G}^{-1}$ with the high-field peak occurring at 3.9 kG. This calculated attenuation is similar to the measured attenuation except for the exact peak position and periodicity. This discrepancy in the period remains unexplained. In Al the majority carriers are the holes and the hole surface does not satisfy the conditions for geometric resonance. It is, therefore, not surprising that geometric resonance was unobserved.

In this analysis we have shown that the longitudinal case ($\mathbf{q} \parallel \mathbf{H}$) is much more complex than the perpendicular case and, notwithstanding the strong attenuation peaks, is unlikely to yield much information about the Fermi surface.

ACKNOWLEDGMENTS

I would like to thank Professor H. Fritzsche for his encouragement and guidance as well as his important suggestions during all phases of this work. I am also indebted to Dr. V. Rehn for his helpful suggestions concerning the experimental aspects of this work, to H. Aubauer who has communicated the results of his work prior to publication, to Professor V. Heine, and to Professor M. H. Cohen for helpful discussions concerning the theoretical aspects of this problem.

I have also profited greatly in discussions with Dr. Y. Eckstein, Dr. J. B. Ketterson, and P. Sievert. I would like to thank Dr. L. Windmiller for the antimony

sample as well as for a report of his results on anti-mony. I am grateful to R. Glosser for the aluminum sample, and to Dr. Stark and to Dr. R. Johnson for their suggestions on sample preparation. I would also like to thank D. Lee for the spectroscopic analysis of the samples. The use of the facilities of the Low Temperature Laboratory supported by the National Science Foundation and the Materials Preparation Laboratory supported by the Advanced Research Projects Agency is gratefully acknowledged.

APPENDIX A

1. Fermi Surfaces Centered on Γ

The conductivity tensor can be written [see Eq. (4.25)] as

$$\sigma^{\pm} = \frac{e^2}{4\pi^3 \hbar^2} \int_{-k_{Fz}}^{k_{Fz}} \frac{m_c}{\omega_c} dk_z \int_0^{2\pi} (v_x \pm i v_y) d\phi \times \int_{-\infty}^{\phi} v_x' K(\phi, \phi') d\phi', \quad (\text{A1})$$

where $K(\phi, \phi')$ is defined in Eq. (4.12). Using the velocity expansions given by Eq. (4.26) valid for s -fold

rotationally symmetric Fermi surfaces about k_z centered on Γ , $K(\phi, \phi')$ can be evaluated and becomes

$$K(\phi, \phi') = \exp \left[i \left(\frac{q \bar{v}_z}{\omega_c} - \frac{\omega}{\omega_c} \right) (\phi' - \phi) \right] + \frac{\phi' - \phi}{\omega_c \tau} - \sum_r c_r \sin(r\phi') + \sum_r c_r \sin(r\phi), \quad (\text{A2})$$

where $c_r = qB_r/\omega_c \tau$, and $c_0 = 0$. Remembering that $\exp[iW \sin\phi] = \sum_m J_m(W) e^{im\phi}$, where J_m is the m th-order integral Bessel function, we can write Eq. (A2) as

$$K(\phi, \phi') = \exp[i(X - \omega/\omega_c)(\phi' - \phi)] \times \prod_r \left[\sum_m J_m(c_r) e^{-imr\phi'} \right] \prod_r \left[\sum_{m'} J_{m'}(c_r) e^{im'r\phi} \right], \quad (\text{A3})$$

where $X = qv_z/\omega_c$ and \prod_r is the product sign. Equation (A3) can be simplified using the identity

$$\prod_r \sum_m R_{mr} = \sum_{m_1} \sum_{m_2} \cdots \sum_{m_r} \prod_r R_{m_r r}$$

and then inserted into Eq. (A1), which after integration over ϕ' yields

$$\sigma^{\pm} = \frac{e^2}{8\pi^3 \hbar^2} \int_{-k_{Fz}}^{k_{Fz}} m_c \tau dk_z \int_0^{2\pi} (v_x \pm i v_y) d\phi \sum_{m_1} \sum_{m_1'} \cdots \sum_{m_r} \sum_{m_r'} \sum_l \left[\prod_r J_{m_r}(c_r) \right] \left[\prod_r J_{m_r'}(c_r) \right] \exp \left[i \sum_r (m_r' - m_r) r \phi \right] \times \left[\frac{e^{i(l+1)\phi} A_{l+1}}{1 + i\omega_c \tau (X - \omega/\omega_c + l + 1 - \sum_r m_r r)} + \frac{e^{-i(l+1)\phi} A_{l+1}}{1 + i\omega_c \tau (X - \omega/\omega_c - (l+1) - \sum_r m_r r)} + \frac{e^{i(l+3)\phi} A_{l+3}}{1 + i\omega_c \tau (X - \omega/\omega_c + l + 3 - \sum_r m_r r)} + \frac{e^{-i(l+3)\phi} A_{l+3}}{1 + i\omega_c \tau (X - \omega/\omega_c - (l+3) - \sum_r m_r r)} \right]. \quad (\text{A4})$$

Finally putting

$$v_x \pm i v_y = \sum_l A_{l+1} e^{\pm i\theta(l+1)\phi} - \sum_l A_{l+3} e^{\mp i\theta(l+3)\phi}$$

into Eq. (A4), σ^{\pm} becomes

$$\sigma^{\pm} = \frac{e^2}{8\pi^3 \hbar^2} \int_0^{k_{Fz}} m_c \tau \sum_a \sum_b \sum_l \sum_{l'} \sum_{m_1} \sum_{m_1'} \cdots \sum_{m_r} \sum_{m_r'} \left\{ A_{l+1} \left(\prod_r J_{m_r} J_{m_r'} \right) (A_{l+1} C_{a,b}^{\pm} + A_{l+3} D_{a,b}^{\pm}) \times \left[\frac{1}{1 + i\omega_c \tau (X - \omega/\omega_c + a(l+b) - \sum_r m_r r)} + \frac{1}{1 + i\omega_c \tau (-X - \omega/\omega_c + a(l+b) - \sum_r m_r r)} \right] \right\} dk_z, \quad (\text{A5})$$

where $a = \pm 1$, $b = 1, 3$, and $l = 0, 4, 8, \dots$, and $r = s, 2s, \dots$ for s -fold rotational symmetry. The constants $C_{a,b}^{\pm}$ and $D_{a,b}^{\pm}$ are

$$C_{a,b}^{\pm} = \begin{cases} 1 & \text{if } a(l+b) \pm g(l'+1) + \sum_r (m_r' - m_r) r = 0 \\ 0 & \text{otherwise} \end{cases}$$

$$D_{a,b}^{\pm} = \begin{cases} 1 & \text{if } a(l+b) \mp g(l'+3) + \sum_r (m_r' - m_r) r = 0 \\ 0 & \text{otherwise,} \end{cases}$$

where $g = +1$ for holes and $g = -1$ for electrons.

When $v_x = \bar{v}_x$, $r=0$ and $c_r=0$ and then $J_{m_r}(0)=0$ except for $J_0(0)=1$. Thus, Eq. (A4) can be evaluated, using the values of $v_x \pm iv_y$ stated earlier, to give Eq. (5.27).

2. Ellipsoidal Fermi Surfaces Not Centered on Γ

For ellipsoidal Fermi surfaces not centered on Γ , the velocity expansion becomes

$$v_x = A \cos\phi, \quad \text{and} \quad v_y = B \sin\phi, \quad \text{and} \quad v_z = \bar{v}_z + c \sin\phi, \quad (\text{A6})$$

written in the coordinate system of the crystal centered on an ellipsoid. Since we are dealing with crystals having 3, 4, or 6-fold rotational symmetry about k_z , there will be n_ϵ ellipsoids about k_z , $2\pi/n_\epsilon$ rad apart, where $n_\epsilon = 3, 4, 6, 8, \text{ or } 12$. The velocities for the other ellipsoids can be obtained by the following axis transformation:

$$v_x^\beta = v_x \cos\left(\frac{2\pi\beta}{n_\epsilon}\right) + v_y \sin\left(\frac{2\pi\beta}{n_\epsilon}\right), \quad v_y^\beta = -v_x \sin\left(\frac{2\pi\beta}{n_\epsilon}\right) + v_y \cos\left(\frac{2\pi\beta}{n_\epsilon}\right), \quad \text{and} \quad v_z^\beta = v_z, \quad (\text{A7})$$

where $\beta = 1, 2, \dots, n_\epsilon$. The conductivity σ^\pm is

$$\sigma^\pm = \sum_\beta \sigma_{xx^\beta} \pm i\sigma_{yy^\beta} = \frac{n_\epsilon e^2}{8\pi^3 \hbar^2} \int_{-k_{zF}}^{k_{zF}} dk_z \frac{m_c}{\omega_c} \left[\int_0^{2\pi} d\phi (v_x \pm iv_y) \int_{-\infty}^\phi v_x' K(\phi, \phi') d\phi' + \int_0^{2\pi} (v_y \mp iv_x) d\phi \int_{-\infty}^\phi v_y K(\phi, \phi') d\phi' \right] \quad (\text{A8})$$

and by using Eq. (A6) and σ^\pm can be evaluated and becomes

$$\sigma^\pm = \frac{n_\epsilon e^2}{32\pi^3 \hbar^2} \int_{-k_{zF}}^{k_{zF}} dk_z m_c \sum_m \left[\frac{(B^2 - A^2) J_m(G) J_{m-2}(G)}{1 + i\omega_c \tau (X - \omega/\omega_c + 1 + m)} + \frac{(B^2 - A^2) J_m(G) J_{m+2}(G)}{1 + i\omega_c \tau (X - \omega/\omega_c - 1 + m)} \right. \\ \left. + \frac{(A \mp B)^2 J_m^2(G)}{1 + i\omega_c \tau (X - \omega/\omega_c + 1 + m)} \frac{(A \pm B)^2 J_m^2(G)}{1 + i\omega_c \tau (X - \omega/\omega_c - 1 + m)} \right], \quad (\text{A9})$$

where $G = qC/\omega_c$ and $X = q\bar{v}_z/\omega_c$. If the ellipsoids are not tilted with respect to the k_z axis, $G=0$ and the only non-vanishing terms are those having J_0 in them, then Eq. (A9) reduces to

$$\sigma^\pm = \frac{n_\epsilon e^2}{8\pi^3 \hbar^2} \int_{-k_{zF}}^{k_{zF}} dk_z m_c \left[\frac{(A \mp B)^2}{1 + i\omega_c \tau (X - \omega/\omega_c + 1)} + \frac{(A \pm B)^2}{1 + i\omega_c \tau (X - \omega/\omega_c - 1)} \right], \quad (\text{A10})$$

which is similar to the result obtained by Kjeldaa.

APPENDIX B

The energy equation for the hole Fermi surface in Sb is

$$\frac{2mE_F}{\hbar^2} = \alpha_{11} k_x^2 + \alpha_{22} k_y^2 + \alpha_{33} k_z^2 + \alpha_{23} k_x k_y \quad (\text{B1})$$

and the energy equation for the electron surface is

$$\frac{2mE_F}{\hbar^2} = \beta_1 k_x^2 + \beta_2 k_y^2 + \beta_3 k_z^2. \quad (\text{B2})$$

The Lorentz force on the holes when $H \parallel z$ is

$$\hbar \dot{\mathbf{k}} = \frac{e}{c} \mathbf{v} \times \mathbf{H} = \frac{e\hbar}{mc} \boldsymbol{\alpha} \cdot \mathbf{K} \times \mathbf{H}, \quad (\text{B3})$$

where

$$\alpha = \begin{pmatrix} \alpha_{11} & 0 & 0 \\ 0 & \alpha_{22} & \alpha_{23} \\ 0 & \alpha_{23} & \alpha_{33} \end{pmatrix}, \quad (\text{B4})$$

using $\mathbf{v} = (\hbar/m)\alpha \cdot \mathbf{k}$. Solving for k we get

$$k_x = k_{x0} \cos\phi, \quad k_y = k_{y0} \sin\phi - \frac{\alpha_{23}}{\alpha_{22}} k_z, \quad k_z = \text{const}, \quad (\text{B5})$$

where $\phi = \omega_c t$ and $\omega_c = eH/mc(\alpha_{11}\alpha_{22})^{1/2}$. The quantities k_{x0} and k_{y0} can be solved for using Eq. (B1) and are given by

$$k_{x0} = \frac{\alpha_{23}}{2\alpha_{22}\alpha_{11}} k_z \left[1 + \frac{1}{2} \left(1 + 4 \left(\frac{\alpha_{22}\alpha_{11}}{\alpha_{23}^2} + \frac{\alpha_{11}\alpha_{22}^2\alpha_{33}}{\alpha_{23}^4} + \frac{8\alpha_{11}\alpha_{22}^2 E_F m}{\hbar^2 \alpha_{23}^4 k_z^2} \right)^{1/2} \right) \right], \quad k_{y0} = \frac{\alpha_{23}}{\alpha_{22}} k_z \left[1 + \frac{1}{2} \left(\frac{8\alpha_{22} E_F m}{\hbar^2 \alpha_{22}^2 k_z^2} - \frac{4\alpha_{22}}{\alpha_{23}} \right)^{1/2} \right]. \quad (\text{B6})$$

Finally, the velocity is

$$v_x = \left(\frac{\alpha_{11}\hbar}{m} \right) k_{x0} \cos\phi, \quad v_y = \left(\frac{\alpha_{22}\hbar}{m} \right) k_{y0} \sin\phi, \quad \text{and} \quad v_z = \left(\frac{\alpha_{23}\hbar}{m} \right) k_{y0} \sin\phi + (\alpha_{33} - \alpha_{23}^2/\alpha_{22}) \frac{\hbar k_z}{m}. \quad (\text{B7})$$

The conductivity is then given by Eq. (A9) where $A = (\alpha_{11}\hbar/m)k_{x0}$, $B = (\alpha_{22}\hbar/m)k_{y0}$, $X = (\alpha_{33} - \alpha_{23}^2/\alpha_{22})(\hbar/m)k_z$, and $G = (q\alpha_{23}\hbar/(m\omega_c))k_{y0}$. The equivalent solution for the electron ellipsoids can be obtained by substituting β_1 for α_{11} , β_2 for α_{22} , and β_3 for α_{33} , and by taking into account the fact that there are three electron ellipsoids per Brillouin zone.

For these orbits where $k_z = 0$ (i.e., geometric resonance condition),

$$k_{y0} = -\frac{1}{\hbar} \left(\frac{2mE_F}{\alpha_{22}} \right)^{1/2}, \quad k_{x0} = -\frac{1}{\hbar} \left(\frac{2mE_F}{\alpha_{11}} \right)^{1/2}, \quad \text{and} \quad G = (q\alpha_{23}/(m\omega_c)) \left(\frac{2mE_F}{\alpha_{22}} \right)^{1/2}.$$

Also, $X = 0$, so that σ^\pm [Eq. (A9)] will be a maximum when $m = \pm 1$, since $\omega_c \tau \approx 100$ at 1 kG. Hence σ^\pm becomes

$$\sigma^\pm = \frac{3}{16} \frac{e^2}{\hbar^2 \pi^3} m_c \frac{2E_F}{m} (\alpha_{11} + \alpha_{22}) \frac{J_1^2(G)}{1 - i\omega\tau} \Delta k_z, \quad (\text{B8})$$

where Δk_z is the band of electrons contributing to the geometric resonance at $k_z \approx 0$.